Russian Chemical Reviews **65** (6) 461 – 478 (1996)
© 1996 Russian Academy of Sciences and Turpion Ltd

UDC 541.16

Ternary carbides and nitrides based on transition metals and subgroup IIIB and IVB elements: electronic structure and chemical bonding

A L Ivanovskii

Contents

I. Introduction 461
II. Chemical bonding and electronic structures of *d*-metal aluminonitrides and aluminocarbides 461
III. Electronic properties of transition metal siliconitrides and silicocarbides 469
IV. Chemical bonding in ternary carbides and nitrides based on subgroup VIIA and VIIIA transition metals 474

Abstract. Data obtained in theoretical and experimental studies on the electronic structures, the nature of chemical bonding, and certain physicochemical properties of ternary carbides and nitrides involving transition metals and subgroup IIIB and IVB elements are surveyed. The possibilities and prospects for the application of computational quantum-chemical methods for the modelling of new complex solid solutions based on metal-like carbides and nitrides and also for the description of their fundamental properties are discussed. The bibliography includes 168 references.

I. Introduction

The high-temperature refractory transition metal (TM) carbides and nitrides and their reciprocal solid solutions (SS) constitute an extensive class of compounds which are interstitial phases.[1-3] By virtue of a unique combination of a series of physicochemical properties, these compounds are exceptionally important.[3-6] Studies on the electronic properties and on the nature of the chemistry bonding in such compounds have made a significant contribution to the development of the quantum chemistry of the solid state. They are being continued vigorously also at the present time. The results obtained in the course of these investigations have been described in numerous publications.[7-12]

The current state of the chemistry and materials science of refractory transition metal carbides and nitrides involves vigorous investigations directed to the improvement of their properties. The properties can be altered by introducing into the composition 'non-traditional' interstitial elements, mainly subgroup IIIB and IVB elements (Al, Si, etc.). The compounds of these elements with carbon and nitrogen are nonisostructural with *d* metal carbides and nitrides, involving predominantly covalent bonding. Such compounds have found a wide variety of application as chemically stable, ultrahard, semiconducting materials[13-15] and they are also convenient objects for the investigation of the electronic structures of solids by computational quantum-chemical methods.[16-21]

The interest in the study of ternary systems of the type M–M′–(C,N), where M is a transition metal and M′ a non-transition subgroup IIIB or IVB element, is associated primarily with the search for new ceramic materials, which are likely to be useful in the development of protective coatings, materials for the manufacture of instruments, and constructional materials and with the creation of new composites and the determination of the possibilities for their employment in microelectronics, and optics, as catalysts, and as elements in reinforced composite materials for space technology.

Studies on the equilibrium phase relations in the M–M′–(C,N) systems have demonstrated[1-5] the existence of an extremely large set of ternary phases. The thin-film technologies,[22-29] which make it possible to produce equilibrium metastable or crystalline and amorphous phases and to vary their microstructure and the content of atomic components over a wide range of concentrations, have therefore assumed a special importance in the creation of new materials. The combination of thin-film technologies with various procedures for the activation of processes involving the preparation of the compositions has led to the possibility of a flexible modification of their physicochemical properties. The problem of the description of the electronic properties of the above multicomponent systems (both mono- and hetero-phase) has become of current interest in this connection. An important place has also been assigned to the determination of specific features of the electronic structure (ES) and the chemical bonding in the individual ternary phases formed in the M–M′–(C,N) systems. The groups of carbides and nitrides having the composition $M_3M'(C,N)$ are of considerable interest in this respect.

The magnetic properties of these carbides and nitrides, in particular the magnetic (and structural) phase transitions, which are of technological importance, have attracted the greatest attention of investigators.[29-32]

In the present review, an attempt has been made to survey available data on the electronic structures and the chemical bonding in the solid solutions and in the ternary carbide and nitride phases based on transition metals and subgroup IIIB and IVB elements, obtained within the framework of computational approaches to solid state quantum chemistry and also with the aid of X-ray emission and X-ray photoelectron spectroscopy.

II. Chemical bonding and electronic structures of *d*-metal aluminonitrides and aluminocarbides

The aluminium-containing phases formed in the M–Al–C, M–Al–N, M–Al–C–N, etc. systems have been most thoroughly investigated among complex carbides and nitrides. A representative group of solid compounds of the type $M_3Al(C,N)$ and $M_2Al(C,N)$, having individual crystal structures[1-4] and

A L Ivanovskii Institute of Solid State Chemistry, The Ural Division of the Russian Academy of Sciences, Pervomaiskaya ul. 91, 620219 Ekaterinburg, Russian Federation. Fax (7-343) 244 44 95.

Received 8 November 1995
Uspekhi Khimii **65** (6) 499 – 518 (1996); translated by A K Grzybowski

between the octahedra. According to estimates,[1,60] the compositions of Ti_2AlC_x and Ti_3AlC_x may vary in the range $0.2 \leqslant x \leqslant 1.2$.

The initial ideas about the possible types of interatomic interactions in the Ti_2AlC_x and Ti_3AlC_x phases were based on the analysis of their crystal-chemical parameters. Thus the Ti–C distance in Ti_3AlC is close to the sum of the covalent radii of titanium and carbon, which makes it possible to postulate[61] the existence of a strong covalent Ti–C bond. On the other hand, the Al–Al distance is much greater than the sum of the covalent radii of aluminium, which discounts the occurrence of direct Al–Al interactions. Similar comparisons of the atomic radii and the interatomic distances for the Ti–Ti, Al–Ti, and Al–C pairs of atoms lead to the conclusion that there is a possibility of the formation of bonds between titanium and aluminium atoms (Ti–Ti, Al–Ti) and that there are no bonds between aluminium and carbon atoms.[61]

A more detailed analysis of the nature of the interatomic interactions in the aluminocarbides Ti_2AlC_x and Ti_3AlC_x has become possible by virtue of the results of studies of their X-ray emission and absorption spectra.[62] It was found that the Ti L_α band in the emission spectrum, reflecting the energy distribution of the d states of the metal, becomes appreciably broadened in the sequence $TiC_x \rightarrow Ti_2AlC_x \rightarrow Ti_3AlC_x$, the main maximum shifting towards the long-wavelength region of the spectrum with simultaneous increase in the intensity of the short-wavelength maximum, which has the same energy as the Al $L_{2,3}$ peak, i.e. the $d(t_{2g})$ states of titanium are filled as a result of the partial transfer of electron density in the Al → Ti direction. This may indicate the hybridisation of the near-Fermi Ti $3d,4s$–Al $3s,3d$ states. The identity of the energies of the long-wavelength Ti L_α and Al $L_{2,3}$ maxima in the emission spectra indicates the appearance of covalent Ti–Al bonds.[62]

With increase in the number of carbon vacancies, the intensity of the low-energy maximum of the Ti L_α band also increases, which is due to the transfer of part of the electron density to the near-Fermi region. Overall, the variable-composition transition metal aluminocarbides may be regarded as phases involving the insertion of carbon into the hypothetical titanium aluminides Ti_2Al and Ti_3Al, the system of interatomic interactions which results in the formation of the Ti–C, Ti–Ti, and Ti–Al bonds.[62] The ionic components of the Ti–C and Ti–Al bonds are due to partial charge transfer in the Ti → C and Al → Ti directions.

More detailed information about the nature of the interatomic structure and the chemical bonding in aluminium-containing carbides and nitrides has been provided by the results of quantum-chemical calculations.[10,12,63–65]

The initial ideas about the specific features of the rearrangement of the electronic state in MC and MN (M = Ti, V, Zr, Nb), associated with the insertion of isolated aluminium atoms in the sublattices of these binary phases (similar systems evidently occur in the initial stage of the syntheses of aluminocarbide and aluminonitride solid solutions and compounds) have been considered,[63] resorting to band and cluster approaches.

The linearised muffin-tin-orbital Green's functions method (LMTO GF) has been used[63,65] to calculate the electronic structures of the MC:Al and MN:Al systems in which single aluminium impurities are inserted at sites within the metallic or nonmetallic sublattices of the matrix with formation of 'microclusters' of the type AlC_6, AlN_6 or AlM_6 (when account is taken of the size factor, this appears most likely) in the bulk of the initial crystal.

In particular, it has been found for the TiC:Al system in the case of Al → Ti substitution that there is now an admixture of the Al $3s$ states at the bottom of the valence band of the monocarbide. The Al $3p$ states form an intense peak near the Fermi energy (E_F) in the region of the minimum of the density of states (DOS) of titanium carbide, i.e. in this instance the impurity–crystal interaction takes place mainly with participation of the Al $3s$–C $2p$ functions with an additional contribution by the hybrid Al $3p$–C $2p$ orbitals.

The pattern in the distribution of the local density of states (LDOS) of the impurity inserted at a C-sublattice site, whereupon the Al $3s$ states are localised near the lower edge of the $p-d$ band of the carbide and their overlap with the valence states of the latter is significant, becomes markedly different. In their turn, the Al $3p$ functions give rise to distinct atom-like resonances in the region of the local DOS minima of the carbide.

A similar pattern in the distribution of impurity states occurs in the TiN:Al system.[65]

Thus an appreciable difference in the energy distributions of the impurity states of the aluminium and the states of the component atoms of the matrix is observed in the MC:Al and MN:Al systems, which indicates significant differences in the nature of the bonds formed by Al with the matrix component atoms and the M–C (or M–N) bonds.[7–12] This is one of the causes of the limited solubility of aluminium in TiC and TiN (in contrast to transition metals).[1,60]

Evidently the presence of local impurity peaks near the edge of the TiC and TiN energy bands, reflecting the states of the aluminium atoms not participating in the formation of the Al–carbide (Al–nitride) bonds, promotes an increase in the number of direct Al–Al interactions with increase in the concentration of aluminium in the bulk of the crystals. Such interactions compete with the system of bonds in carbides and nitrides. As a result, the structural type of the initial matrix changes because of the formation of phases with an individual type of crystal structure, which has in fact been observed experimentally.[60]

The partial interatomic interactions in the TiN:Al system have been analysed[66] within the framework of the nonempirical discrete variation method.[67,68] The parameters of the photoelectron spectrum and the populations of the interatomic bonds of the $TiN_6Ti_{12}N_8$ and $AlN_6Ti_{12}N_8$ fragments, modelling $TiN_{1.0}$ and TiN:Al respectively, have been compared. The overlap integrals (OI) of the atomic wave functions obtained for the above fragments indicate that the interatomic bonds are based on the Ti $d(e_g,t_{2g})$–N $2p_{x,y,z}$ interactions (of the σ and π types). The introduction of aluminium atoms diminishes somewhat the maximum values of the Ti–N overlap integrals (c ranges from approximately 0.300e to 0.296e for the $TiN_6Ti_{12}N_8$ and $AlN_6Ti_{12}N_8$ groups respectively), the Al–N interaction occurring as a result of the overlap of the Al $3s,3p$–N $2p$ functions.

The electronic properties of a series of hypothetical ordered $Ti_xAl_{1-x}N$ ($x = 0.75$, 0.50) cubic solid solutions have been investigated by the self-consistent linearised augmented plane waves (LAPW) method.[69,70] The unit cell of the model structure of the $Ti_{0.75}Al_{0.25}N$ ($Ti_3AlN_3^{[4]}N^{[6]}$) phase contained a nitrogen atom ($N^{[6]}$) involved in a regular Ti_6 octahedral coordination and $N^{[4]}$ type atoms with a Ti_4Al_2 in closest proximity. The cell used for the description of the $Ti_{0.5}Al_{0.50}N$ ($TiAlN^{[2]}N^{[4]}$) composition is formed on the basis of the cubic cell by the displacement of the titanium atoms in its upper and lower planes by aluminium atoms.

The principal characteristics of the electron spectra of both phases are presented in Fig. 3 and Table 3. Comparison with the data obtained with the $TiN_{1.0}$ electron spectrum[71–74] shows that the aluminonitride alloys on the whole retain the principal features of the spectrum characteristic of titanium mononitride: the Ti_xAl_yN valence band contains an isolated low-energy band made up predominantly of the nitrogen $2s$ states (the s band) and separated by the forbidden gap (FG) from the main valence-bonding band (the $p-d$ band). Partial Ti → Al replacement leads to a narrowing of the s band (by 0.08 Ry for $Ti_{0.50}Al_{0.50}N$ compared with $TiN_{1.0}$) and of FG (by 0.18 Ry); on the other hand, the $p-d$ band, partially overlapping the bands of the near-Fermi Ti d states, is broadened (as a consequence of the admixture of the aluminium s,p valence states).

Compared with $TiN_{1.0}$,[71–74] the DOS distribution for aluminonitrides[60,70] does not exhibit significant differences in the region of the s and d subbands. The most notable DOS rearrangement, arising due to the appearance of new DOS peaks near the

Table 3. The results of LMPW calculations for the $Ti_{0.75}Al_{0.25}N$ and $Ti_{0.50}Al_{0.50}N$ ordered cubic phases.

Parameter	$Ti_{0.75}Al_{0.25}N$	$Ti_{0.50}Al_{0.50}N$
Lattice constant / a.u.		
a	7.9841	5.5988
c	—	7.9179
Radii of atomic spheres / a.u.		
Ti, Al	2.1206	2.1031
N	1.8714	1.8559
Band width / Ry		
s	0.224	0.265
p	0.576	0.600
d (occupied)	0.166	0.162
Width of the *s*–*p* interband gap / Ry	0.282	0.279
E_F (relative to bottom of *s* band) / Ry	1.247	1.305
E_F (relative to muffin-tin zero) / Ry	0.841	0.871

Table 4. The effective atomic charges (e) for $TiN_{1.0}$, $Ti_{0.75}Al_{0.25}N$, and $Ti_{0.50}Al_{0.50}N$.

Phase	Ti	$N^{[6]*}$	$N^{[4]}$	$N^{[2]}$	Al
$TiN_{1.0}$	−0.33	0.38	–	–	–
$Ti_{0.75}Al_{0.25}N$	−0.27	0.36	0.38	—	−0.43
$Ti_{0.50}Al_{0.50}N$	−0.24	–	0.39	0.41	−0.39

Note. The effective atomic charges were determined as the differences between the charges in the atomic spheres according to the LAPW calculations and the superposition of the charge densities of the atoms in the crystal.

upper and lower edges of the given subband, is observed in the region of the *p*–*d* band of the nitride.

The densities of states of the $N^{[6]}$ atoms, having the Ti_6 environment, are similar to those for nitrogen in $TiN_{1.0}$[74] and are determined by the σ-bonds (p–d_{z^2} overlap) and π-bonds (overlap of p–d_{xz}, d_{yz} orbitals). The $N^{[4]}$ p_z orbitals are oriented towards the aluminium atoms and form DOS peaks in the region of the localisation of the energies of the Al 3*s*,3*p* states, which indicates the occurrence of the $N^{[4]}$–Al(p_z–s,*p*) interactions. The highest-energy peak of the $N^{[4]}$ p_z states is due to the partial transfer of electron density from the nearest surrounding nitrogen atoms to the atomic sphere of the aluminium.

The distribution of the local density of states of $Ti_{0.50}Al_{0.50}N$ repeats overall the situation examined above with the exception of certain features[70] associated with the decrease in the symmetry of the system as a consequence of the increase in the Al : Ti ratio.

Analysis of the partial charges in the atomic spheres presented in Table 4 shows that the charge polarisation in aluminonitrides leads to a partial shift of electron density (ED) in the (Ti,Al) → N direction, which agrees with the XPES data and the results of cluster calculations by the discrete variation method.[35, 54, 66]

The features noted above in the distribution of the charge densities and interatomic interactions are clearly illustrated by the maps of the electron density distribution (Fig. 4). Comparison of Figs 4*a* and 4*b* shows that the σ(Ti–N)-bond in the $Ti_{0.50}Al_{0.50}N$ phase is somewhat stronger than in the $Ti_{0.75}Al_{0.25}N$ phase. This is also true of the π-type Ti–Ti bonds. Furthermore, the distribution

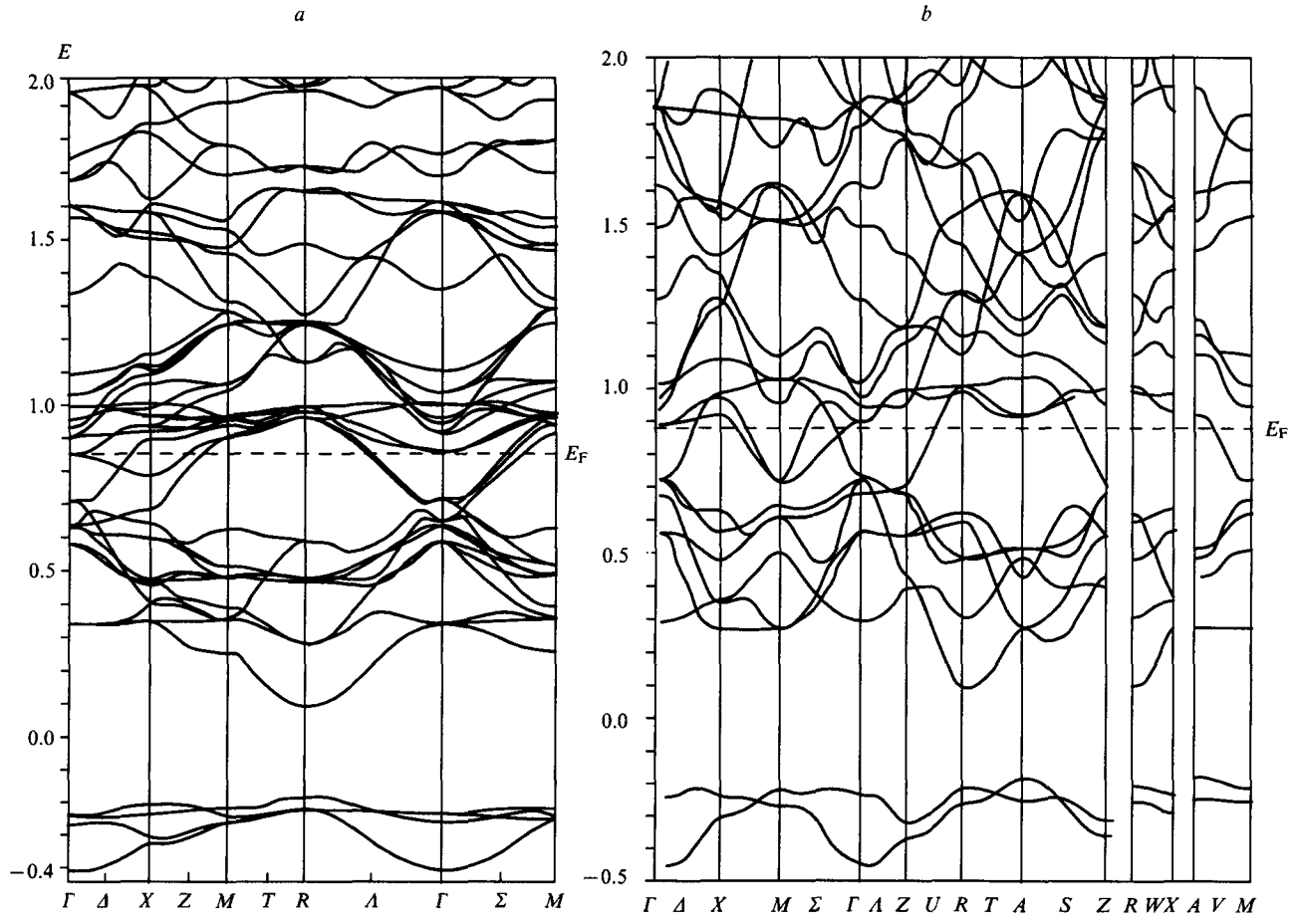


Figure 3. The energy bands of the hypothetical ordered aluminonitrides $Ti_{0.75}Al_{0.25}N$ (*a*) and $Ti_{0.50}Al_{0.50}N$ (*b*); calculation by the LAPW method.

of the maxima in the contours of the $d(e_g)$ orbitals indicates the possibility of Ti–Al bond formation and the appreciable density of the lines around the atomic nuclei of aluminium indicates the presence of an ionic component of the bond.

It was noted previously that the cubic aluminonitride alloys synthesised are characterised by configurational disorder in the metallic sublattice. An attempt has been made [69,75] to take this factor into account. The calculation was performed within the framework of the Korringa–Kohn–Rostocker coherent potential approximation (KKR CPA) method; the concept of an effective medium, simulating the average configuration of the system, has been introduced for the description of disordered systems.[76] Since the calculations [69,75] were nonself-consistent, the potentials of the atoms of the disordered $Ti_xAl_{1-x}N$ ($x = 0.75$, 0.50) alloys were taken from calculations of regular structures by the LAPW method [70] and were averaged for atoms of one kind.

Fig. 5 presents as an example the local densities of states for aluminium in the ordered and disordered aluminonitrides. Evidently, allowance for disorder in the metallic sublattice is manifested mainly (with retention of the overall sequence in the energy distributions of the *s,p,d* functions of aluminium in the spectrum) by the 'spreading' of a series of peaks in the LDOS spectrum of the regular structure. Furthermore, the noncoincidence of the maxima of the Al 3*s* subband, calculated by the KKR CPA and LAPW methods, has been noted,[75] while the bottom of the band for the ordered alloy is ~1 eV deeper than for the disordered alloy with a statistical distribution of the Ti and Al atoms at the corresponding sublattice sites.

The specific features of the fitting of the coherent potential approximation are known [77] to preclude a detailed consideration of the mechanism of chemical bonding. The LDOS obtained were therefore used[75] for the theoretical calculation of the form of the X-ray emission, photoelectron, and Auger electron spectra. The Al K_α emission lines plotted (within the framework of the formalism of the dipolar approximation [77,78]) for $Ti_{0.75}Al_{0.25}N$ and $Ti_{0.50}Al_{0.50}N$ are presented in Fig. 5. Estimates [69] of the transition matrix elements make it possible to interpret the form of the *L* spectrum of aluminium as a superposition of its *s* and *d* states. The *L* band in the aluminium spectrum (as for the wurtzite-like AlN) [79] contains three maxima, but the ratios of their intensities are markedly different, while the energy gaps between the maxima for $Ti_{0.75}Al_{0.25}N$ are greater than those for AlN by ~0.9 eV. Furthermore, in contrast to aluminium nitride,[79] the Al *N* and Al *K* line maxima do not have the same energies. The aluminium *K* bands undergo the greatest changes (with a relative stability of Al *L* line) associated with the variation of the Al/Ti ratio.

The photoelectron spectra of Ti_xAl_yN have been calculated [77,80,81] by a standard method for the photon energies $E = 1487$ and 150 eV. The theoretical integral Auger spectra were also plotted (Fig. 5) as convolutions of the corresponding partial states of the aluminonitrides.[82,83] In particular, it was noted that the form of the Ti $L_2M_{23}V$ line is determined by the distribution of the *p* and *d* states of titanium.

Comparative analysis of the stability of the cubic titanium aluminocarbides and aluminonitrides as a function of the site of substitution (Al → Ti or Al → C,N) and also of the aluminium content in the initial TiC and TiN has been carried out [84–86] within the framework of the LMTO method in terms of the atomic sphere approximation (ASA).[87]

Using the Ti_4X_4 (X = C, N) supercell, the Ti–Al–N and Ti–Al–C solid solutions having the following compositions have been modelled with the aid of the successive substitution of titanium or nonmetal atoms by aluminium atoms: TiN, $Ti_{0.75}Al_{0.25}N$, $Ti_{0.50}Al_{0.50}N$, $TiAl_{0.25}N_{0.75}$; TiC, $Ti_{0.75}Al_{0.25}C$, $Ti_{0.50}Al_{0.50}C$, $TiAl_{0.25}C_{0.75}$.

The results of the calculations of the electronic structure of $Ti_xAl_{1-x}N$ by the LMTO [84–86] and LAPW [70] methods agree satisfactorily. A significantly different type of DOS and LDOS has been obtained [84,86] for the $TiAl_{0.25}N_{0.75}$ solid solution, where

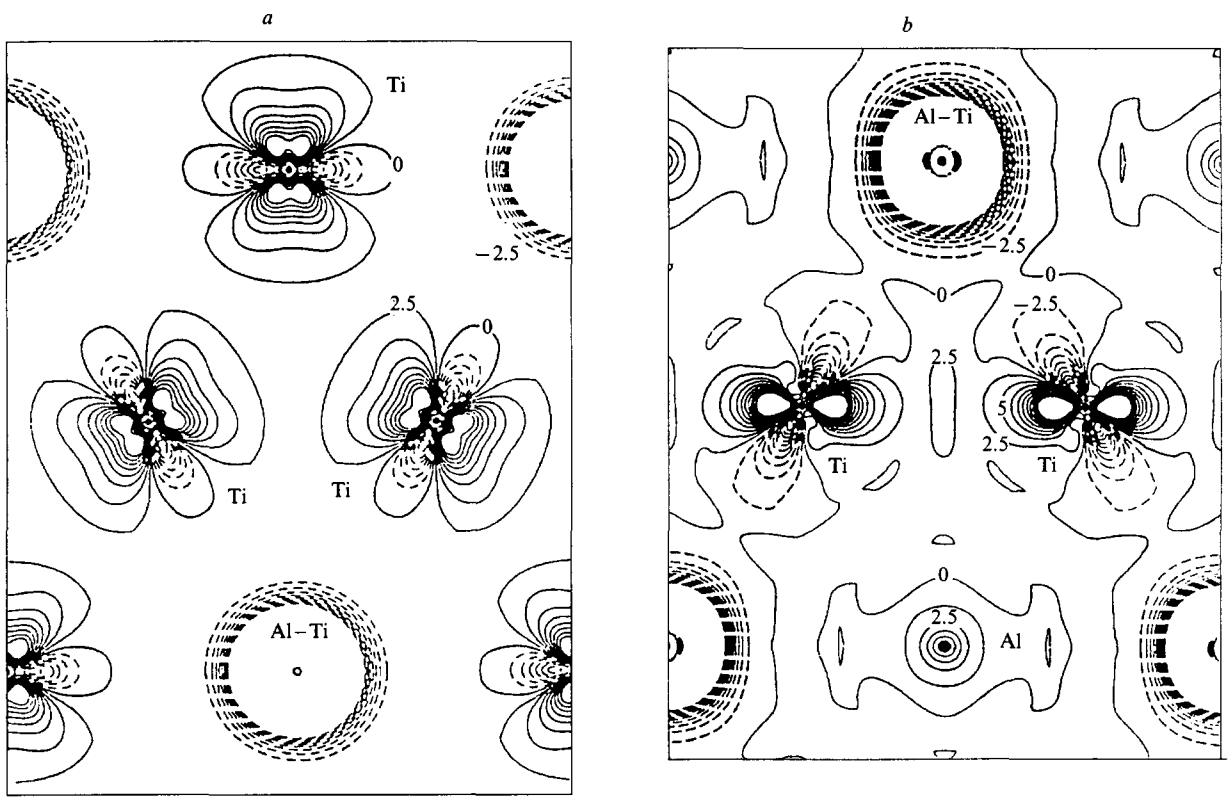


Figure 4. Maps of the differential electron density in the (111) plane of the $Ti_{0.75}Al_{0.25}N$ and $TiN_{1.0}$ phases (*a*) and of the $Ti_{0.50}Al_{0.50}N$ and $Ti_{0.75}Al_{0.25}N$ phases (*b*). The numerals on the curves denote the electron densities; the electron density between the contours is 0.01 e Å^{-3}; calculation by the LAPW method.

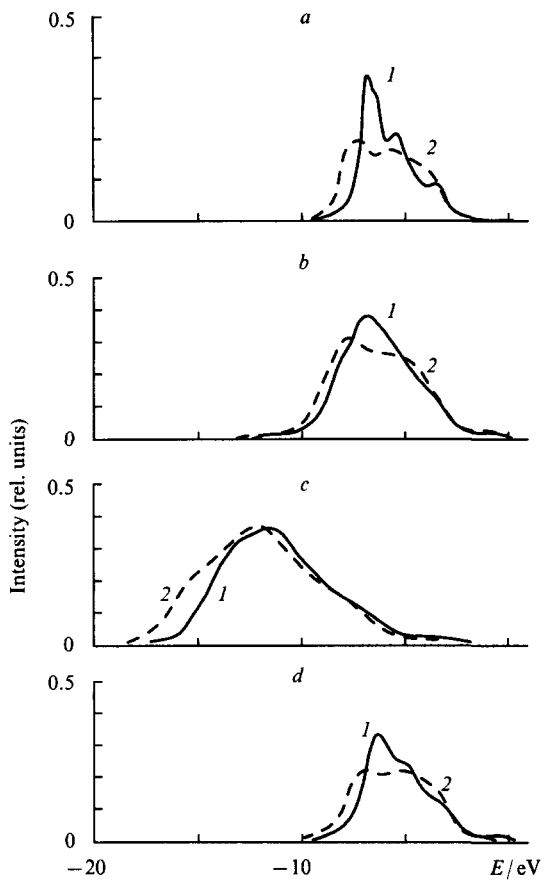


Figure 5. The distribution of the Al 3*p* states (*a*), the theoretical forms of the Al $KL_{2,3}V$ (*b*) and Al *KVV* (*c*) Auger electron spectra, and the form of the Al K_α line (*d*) in the X-ray emission spectra for the $Ti_{0.75}Al_{0.25}N$ (*1*) and $Ti_{0.50}Al_{0.50}N$ (*2*) phases. Calculation by the KKR CPA method.

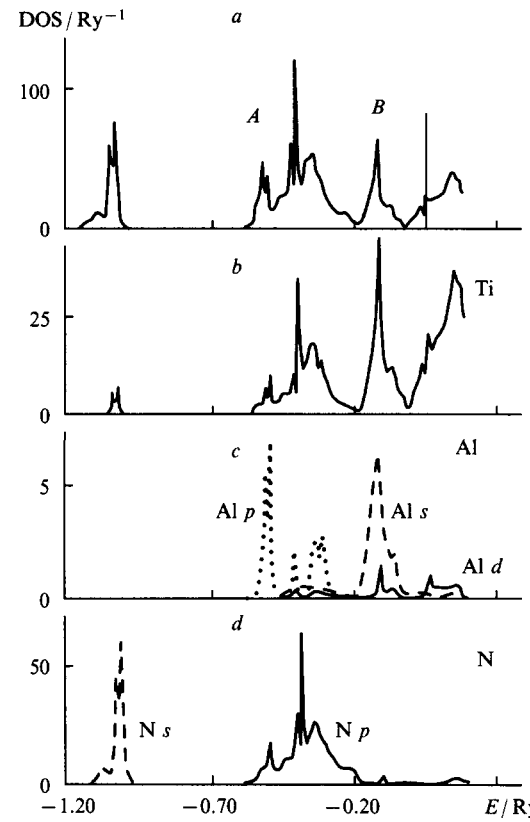


Figure 6. The total (*a*) and partial (*b*–*d*) DOS for the cubic $TiAl_{0.25}N_{0.75}$. Calculation by the LMTO method.

the insertion of the aluminium atoms at the N-sublattice sites was postulated (Fig. 6).

The most characteristic difference between the $TiAl_{0.25}N_{0.75}$ and $Ti_xAl_{1-x}N$ spectra is the sharp increase in the energies of the Al 3*s* and Al 3*p* states: the energies of the Al 3*s* state range from −0.55 to −0.52 Ry (peak *A* in Fig. 6; the lower edge of the *p*–*d* band), giving rise to an intense atom-like resonance, while the energies of the Al 3*p* states (peak *B* in Fig. 6) correspond to the region of the DOS minimum for the nitride between the *p*–*d* and *d* bands. The forms of the N 2*s* and N 2*p* local densities of states remain similar to those in the nitride under these conditions (the immediate environment of aluminium in the given solid solution is $AlTi_6$), which may be attributed to the local character of the interatomic interactions occurring in the solid solutions under discussion.

The dissociation of some of the Ti–N bonds in $TiAl_{0.25}N_{0.75}$ (on replacement of N atoms by Al) results in the transition of a series of titanium states to a higher-energy region [between the *p*–*d* and *d* bands, the LDOS peak of titanium (Fig. 6) has the same energy as peak *B* of the density of states of $TiAl_{0.25}N_{0.75}$] where the Al 3*p*,3*d* states are also located. As a result, in contrast to the solid solutions $Ti_xAl_{y-x}N$, in which the bonding of the aluminium atoms is achieved via the Al 3*s*,3*p*–N 2*p* hybridisation, in the hypothetical solid solution $TiAl_yN_{1-y}$ the bonding of aluminium takes place primarily as a result of the mixing of the Al 3*p*,3*d*–Ti 3*d*,4*s* functions.

The LMTO calculations[84,86] for the electronic states of the cubic (*B*1) solid solutions $Ti_xAl_{1-x}C$ and $TiAl_xC_{1-x}$ show that, as for the aluminonitride alloys, the LDOS distributions for the component atoms in these solutions differ markedly depending on the sites occupied by the aluminium atoms. Thus, for the substitution of the Ti → Al type, the impurity states are located in the region of the C 2*s* and *p*–*d* bands of the carbide; the occurrence of impurity resonances in the region of the local minima in the density of states in the *p*–*d* band of $TiC_{1.0}$ and between the *p*–*d* and *d* bands is characteristic of the $AlTi_6$ coordination.

Furthermore, with increase in the aluminium content (with decrease in the concentration of the valence electrons), E_F for $Ti_xAl_{1-x}C$ shifts, as for $Ti_xAl_{1-x}N$, to the region of low energies. However, the nature of the change in the filling of the valence band for these two groups of solid solutions is fundamentally different: in the case of $Ti_xAl_{1-x}N$ the band of the antibonding delocalised Ti *d*,*s*,*p* states is 'emptied', whereas in the case of $Ti_xAl_{1-x}C$ the filling of the band of the bonding *p*–*d* states diminishes.

The above effect as well as the energy required to 'dissociate' the Ti–(N,C) bonds (for the Ti → Al substitution mechanism) can be attributed[65] to the relative stability of the cubic titanium aluminonitrides and aluminocarbides. Numerous calculations have shown[8–11] that the Ti–C bond energy is much higher than the Ti–N bond energy. Taking into account the nature of the variation of the filling of bands of different nature noted above for the carbide and nitride phases and also the smaller energy expenditure required for the dissociation of the Ti–N bonds, it was concluded qualitatively[64,65] that the probability of the formation of single-phase cubic alloys is higher in the Ti–Al–N system than in the Ti–Al–C system.

In order to confirm this hypothesis, calculations of the cohesion energy (E_{coh}) (i.e. the atomisation energy), of the energy of the substitution (E_{sub}) of titanium (or C, N) by aluminium, and the partial pressures of the electronic-nuclear system of the crystals (p_i) were carried out by the LMTO method.[64,66] The energies E_{coh} and E_{sub} are presented in Table 5. Evidently the absolute value of the cohesion energy for the $Ti_xAl_{1-x}N$ solid solutions diminishes with increasing aluminium content; in the presence of identical aluminium concentrations, $|E_{coh}|$ for

$Ti_{0.75}Al_{0.25}N$ is greater than that for $TiAl_{0.25}N_{0.75}$. Similar relations have been obtained also for substitution energies. From the foregoing, one may conclude that, firstly, the synthesis of homogeneous cubic aluminium-containing solid solutions under equilibrium conditions is difficult (the solutions have been obtained mainly in a metastable state — in the form of films [35-48]); secondly, the probability of the formation of solid solutions diminishes with increasing aluminium content; thirdly, for equal concentrations of aluminium, the substitution by the latter of Ti sublattice sites is energetically more favourable.

Table 5. The cohesion and substitution energies for the aluminium-containing solid solutions based on TiC and TiN.

Compound	$-E_{coh}$ / Ry	E_{sub} / Ry
TiC	1.588	–
$Ti_{0.75}Al_{0.25}C$	1.452	0.136
$Ti_{0.50}Al_{0.50}C$	1.316	0.272
$TiAl_{0.25}C_{0.75}$	1.379	0.209
TiN	1.327	–
$Ti_{0.75}Al_{0.25}N$	1.224	0.103
$Ti_{0.50}Al_{0.50}N$	1.062	0.265
$TiAl_{0.25}N_{0.75}$	1.185	0.142

Similar conclusions [65,66] follow also from the analysis of the energies E_{coh} and E_{sub} for the Ti–Al–C system (Table 5). By comparing the above quantities for the aluminocarbides and aluminonitrides having the same compositions and structures, one may claim that, since $|E_{coh}|$ for Ti–Al–C is greater than that for Ti–Al–N whereas E_{sub} for Ti–Al–N is greater than that for Ti–Al–C, the formation of stable cubic titanium aluminonitrides is more probable.

These conclusions have been confirmed [64] also by the comparison of the pressures p_1. The highest values of $|p_1|$ for TiC and TiN correspond to the (C,N) 2*p* and Ti 3*d* states, the hybridisation of which determines the nature of the chemical bonding in the binary phases.[8-11] When aluminium atoms are inserted at the Ti sites the Ti–(C,N) bonds are somewhat weakened [the quantities $|p_1(Ti)|$ diminish], but some new bonds of the type (N,C)–Al arise as a result of the interaction of the (C,N) 2*p*–Al *s*,*p*,*d* states. Such bonds proved to be much stronger than the Ti–Al bonds formed when aluminium is inserted at nonmetallic sublattice sites. Finally the bonding (negative) pressure of the aluminium states is higher for the nitride alloys than for the carbide-based solid solutions, which again indicates a greater stability of the cubic aluminonitride solid solutions.

The synthesis of aluminium-containing solid solutions involving IVA–VIA subgroup *d* metals, for example, $(TiAlZr)N_x$, $(ZrAl)N_x$, and $(TiAlV)N_x$, has been reported.[23,36,37] However, there is at present no information about their electronic-energy spectra.

In conclusion of this section, we shall mention again those studies [64,65] in which the cluster semiempirical LCAO method was used to analyse the energies of the molecular orbitals (MO) of the clusters, simulating the nonstoichiometric (with respect to the nonmetallic sublattice) *H*- and perovskite-like titanium aluminocarbides and aluminonitrides. In conformity with the available X-ray emission data (see above), it has been established, in particular, that, in the overall system of the Ti_2AlC_x molecular orbitals, it is possible to distinguish four groups, consisting predominantly of the contributions of the C 2*s*, Al 3*s*, C 2*p*–Ti 3*d*–Al 1*s*,*p*, and Al *s*,*p*–Ti 3*d* states. The differences between the formula compositions and the crystal structures of the aluminocarbide phases determine the relative change in the line widths and energies of the individual subbands of the Ti_3AlC and Ti_2AlC valence spectra.

The formation of carbon vacancies leads [65] to the progressive filling of the delocalised near-Fermi Ti 3*d* and Al 1*s*,*p* states and also to some decrease in the contribution of the C 2*p* orbitals to the hybrid band of the Ti 3*d*–C 2*p*–Al 3*s*,3*p* type and to a narrowing of the quasi-core C 2*s* band. Similar relations are observed also in the transition $Ti_2AlN \rightarrow Ti_2AlN_x$ ($x < 1$).

Narrowing and low-energy shifts of the metalloid *s*,*p* sub-bands are characteristic of aluminonitrides (compared with aluminocarbides). The energy separation of the Ti *d*–N *p* states leads to the virtually complete absence of contributions by the latter to the subband of the Ti–Al states, the population of which increases (as a consequence of the increase in the electron concentration per unit cell of the compound).

The overlap populations (OP) of the atomic orbitals and the bond indices [bond populations (BP)] in the case of the fragments for which calculations have been made indicate that the chemical bonding in the *H*-phases is based on Ti–(C,N), Ti–Al, Ti–Ti-type interactions, comparable in terms of BP, and on the interactions of nontransition metals with one another, whereas the bonds between the atoms of nontransition metals and metalloids are virtually absent (Table 6). The Ti–C and Ti–N bond populations in Ti_2AlC and Ti_2AlN are much smaller than in titanium carbides and nitrides, which is evidently the main reason for the reduced hardness and thermal stability of the aluminocarbides compared with titanium carbides.[1,61,62]

The relative bond populations depend on the number of vacancies: when nonmetal defects are introduced, the interlayer interactions are weakened and the bonds in the aluminium layer are strengthened. Individual Ti–(C,N) bonds are weakened (in contrast to the bonds in the cubic TiC_x and TiN_x,[9,10] where the formation of vacancies strengthens some of the remaining metal–nonmetal bonds). An appreciable anisotropy of the individual interactions in the layers near the defect arises; the occurrence of a weak direct Ti–Ti interaction through the carbon or nitrogen layer is observed.

Table 6. Results of calculations by the LCAO MO method of the overlap populations of the valence atomic orbitals (e) for the clusters in the structures of titanium aluminocarbides and aluminonitrides.

Orbital	Al *s*	Al *p*	(C, N) *s*	(C, N) *p*
	Compound Ti_2AlC, cluster $TiAl_3C_6Ti_9$			
Ti *s*	0.06	0	0.11	0.03
Ti *p*	0.08	0.02	0.06	0.02
Ti *d*	0.06	0.02	0.04	0.34
	Compound Ti_2AlC_x, cluster $TiAl_3C_4\square_2Ti_9$ [a]			
Ti *s*	0.05	0.02	0.11	0.05
Ti *p*	0.06	0.01	0.05	0.05
Ti *d*	0.07	0.03	0.04	0.22
	Compound Ti_2Al_2N, cluster $TiAl_3N_6Ti_9$			
Ti *s*	0.08	0	0.09	0.03
Ti *p*	0.14	0.01	0.05	0.04
Ti *d*	0.09	0	0.03	0.23
	Compound Ti_2AlN_x, cluster $TiAl_3N_4\square_2Ti_9$ [a]			
Ti *s*	0.11	0	0.09	0.04
Ti *p*	0.05	0.04	0.03	0.05
Ti *d*	0.11	0.02	0.03	0.20
	Compound Ti_3AlC, cluster $TiAl_4C_2Ti_8$			
Ti *s*	0.03	0.02	0.05	0.06
Ti *p*	0	0	0	0
Ti *d*	0.05	0.03	0.03	0.11
	Compound Ti_3AlC_x, cluster $TiAl_4C\square Ti_8$ [a]			
Ti *s*	0.02	0.06	0.04	0.06
Ti *p*	0	0	0	0
Ti *d*	0.02	0.06	0.03	0.10

[a] The symbol □ denotes vacancies in the C or N sublattices.

On passing from the carbon-containing to the nitrogen-containing phases, the Ti–nontransition metal bonds and the bonds in the aluminium layers are strengthened, primarily as a result of the weakening of the Ti–nonmetal bonds.

It follows from the data[64,65] that the transition metal atoms have an effective positive charge in all the phases considered, which increases on passing from the carbide to the nitride phases. Finally analysis of the overlap integrals between the atomic orbitals shows[65] that the Ti–(C,N) interaction in the *H*-phases takes place, as in the binary carbides and nitrides mainly as a result of the hybridisation of the Ti $3d$–(C,N) p states. The Ti–Al bonds are of a mixed character, involving predominantly the Al s,p states hybridised with all the valence orbitals of titanium.

III. Electronic properties of transition metal siliconitrides and silicocarbides

Yet another class of objects, for which quantum-chemical studies of the electronic-energy spectra and of the nature of the chemical bonds have been initiated and are developing vigorously, comprises transition metal siliconitrides and silicocarbides. Together with aluminium-containing compounds, these substances are of great interest for the manufacture of new ceramic materials, including constructional ceramics. Preliminary investigations[88–94] of ceramics based on transition metal and silicon carbides and nitrides have demonstrated particularly their potential suitability in manufacturing technology at high temperatures.

The first information about the electronic states of the atomic components in phases based on the M–Si–C systems was obtained[95] by the LMTO GF method. This method has been used to calculate the LDOS for isolated atoms of aluminium and the entire series of $3d$ metals which are incorporated at the Si sublattice sites of cubic silicon carbide. These objects were regarded as models and the process involving the incorporation of the atoms M was considered to be a stage leading to the formation of hypothetical solid solutions in the M–Si–C systems, which retain the initial sphalerite-like structure of silicon carbides. In addition, they can simulate one of the probable mechanisms of the formation of intermediate layers in complex silicon-containing ceramics at the contact boundary between a solid grain (SiC) and the elements of the plasticiser, which consist as a rule of d,p metals or their alloys.

The results obtained are presented in Fig. 7. Taking into account the data obtained by band calculations for the ideal $3C$-SiC carbide,[96–101] it was found that the form of the LDOS for the transition metals at the beginning of the $3d$ series is determined by the nature of the overlap of their outer states with the valence band of the matrix. As the orbital energies of the impurity decrease (Sc → Cu), the filled part of the LDOS undergoes a low-energy shift. For M = Mn, the impurity states are concentrated in the region of the local minimum in the density of states in the *pp* band of SiC, whereas for M = Fe, Co or Ni atom-like (nonbonding) LDOS resonances arise in the forbidden gap between the *ss* and *pp* bands of silicon carbide.

The distributions of the lowest free states of the doping d atoms are also found to be significantly different. Their concentration near the upper boundary of the forbidden gap of the carbide increases sharply with increase in the atomic number of the impurity. The nickel impurity exerts the most 'dramatic' effect on the conducting properties of SiC, its presence being responsible for the appearance of resonance peaks in the forbidden gap of silicon carbide.[95]

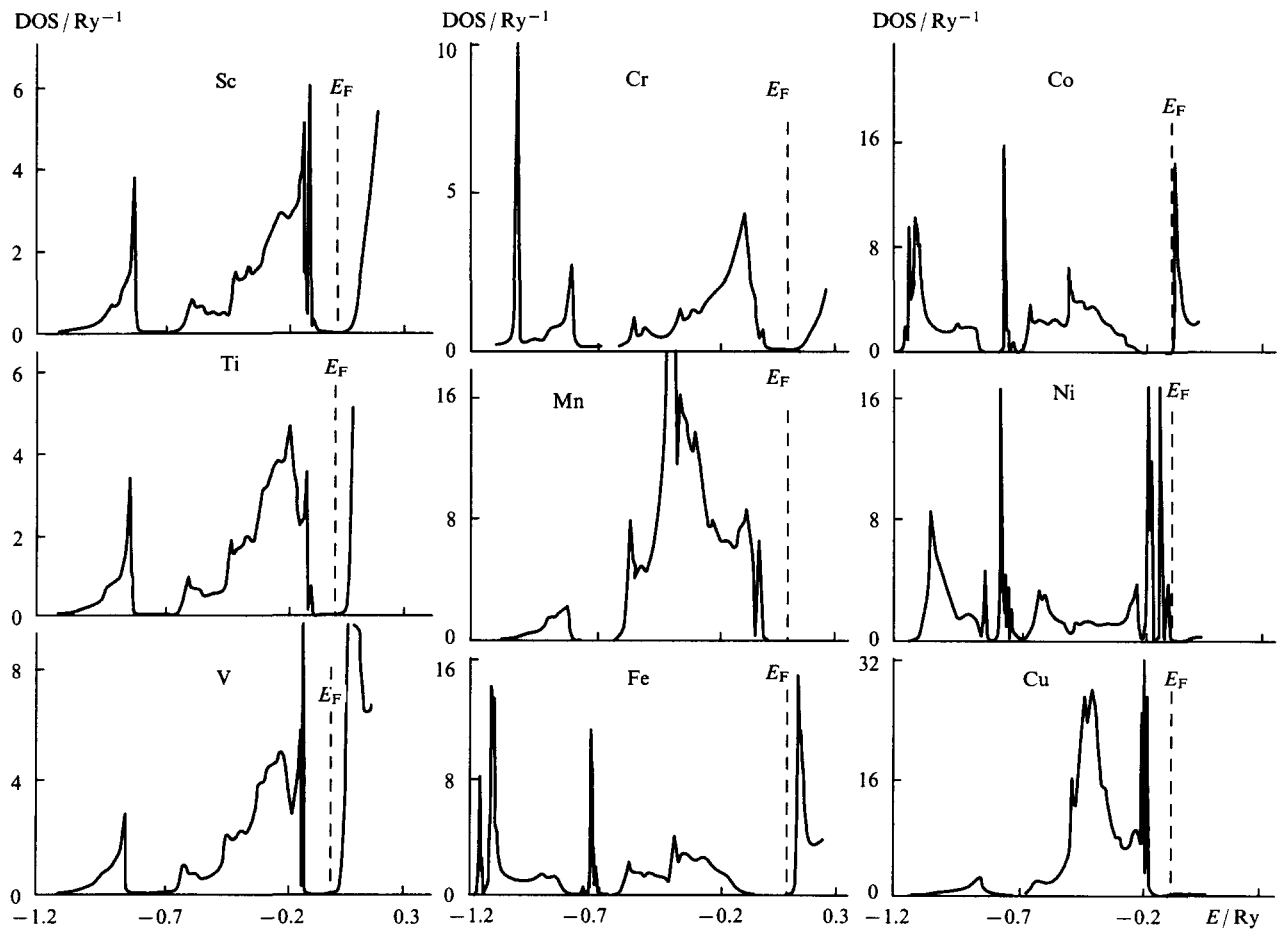


Figure 7. Local DOS of the $3d$ metal impurities in cubic $3C$-SiC. Calculation by the LMTO GF method.

Estimation of the energy characteristics of the rearrangement of the interatomic interactions under the influence of the impurity (by the method proposed in the study of Anisimov et al.[102]) indicates that in all cases the change in the total energy of the initial crystal is positive ($\Delta E > 0$), i.e. the 'rupture' of the stronger Si–C bonds is not compensated by the newly formed M–C bonds and in this respect the systems under consideration proved to be unstable. Minimal destabilisation occurs when the atoms of aluminium and of the 3*d* metals at the beginning and end of the series are introduced into the bulk of silicon carbide. It follows from the foregoing that the formation of the modelled homogeneous solid solutions, retaining the SiC structure, is more difficult[95] than, for example, the formation of reciprocal solid solutions of transition metal carbides and nitrides.[1-7]

The study of M → Si substitution for a 25% concentration of titanium and vanadium impurities in 3*C*-SiC, which exert the least destabilising effect on the energetics of the system under consideration, has been continued[103,104] by the LMTO method. The initial carbide was described using the Si_4C_4 supercell in which the silicon atoms were replaced by titanium or vanadium atoms. This made it possible to calculate the electronic properties of the $Si_{0.75}Ti_{0.25}C$ and $Si_{0.75}V_{0.25}C$ ternary systems. It has been noted that the titanium and vanadium impurities lead to the appearance of sharp DOS peaks in the region of the top of the valence band and alter significantly the form of the DOS of the conductivity band of silicon carbide. These changes are caused by the 3*d* orbitals of the metal, to which corresponds a large negative pressure of the electronic-nuclear system (p_1), i.e. they are bonding in character. For $Si_{0.75}Ti_{0.25}C$, the energy of the substitution of 25% of the silicon atoms by titanium (E_{sub}) is negative, which indicates the possibility of the formation of a stable structure in the Si–Ti–C system, where the titanium atoms occupy silicon sites.

For $Si_{0.75}V_{0.25}C$, the substitution energy is positive. This may be associated both with the differences in the energetics of the formation of bonds by vanadium and titanium with the environment [$|p_1|$(Ti) > $|p_1|$(V)] and with the overall decrease in the cohesion energy of the carbide crystal with the vanadium impurity as a result of the increase in the overall electron concentration.

The possibility of the partial substitution by titanium atoms of the silicon carbide C-sublattice sites has been considered.[104] It was established that the doping of the nonstoichiometric (with respect to carbon) SiC_x with titanium has a negative effect on the overall stability of the system.

The nitrogen impurity has a significantly different effect in this respect. LMTO calculations for the silicon carbonitride $SiC_{0.75}N_{0.25}$ have shown[104] that, on partial C → N substitution, the substitution energy is 0.09 Ry, whereas after application of corrections for dissociation (0.10 Ry) the substitution energy becomes negative.[105,106] Consequently such substitution may be energetically favourable. We may note that a similar small deviation from the linear variation of E_{sub} has been found also for titanium carbonitride.[106]

The results obtained in the syntheses and in the study of the electronic states of yet another group of silicon-containing solid solutions with a different (cubic, of the NaCl type) structure of titanium siliconitrides and silicocarbides have been published in a series of communications.[85,107-109] Films of $Ti_xSi_yN_z$ solid solutions were deposited on a molybdenum foil substrate and on the (100) surface of a NaCl crystal.[109] The composition of the solid solution and the structure and chemical state of the component atoms were investigated as a function of the pressure of the working gas (N_2), temperature, and the potential of the substrate and the cathodic current. With increase in p_{N_2} the nitrogen content in the film increases up to saturation, while the oxygen concentration actually diminishes. The observed type of variation of the N:Ti and O:Ti ratios with nitrogen pressure (Fig. 8) is typical for MN films (M is a transition *d* metal). At lower nitrogen pressures, the variation of the Si:Ti ratio is

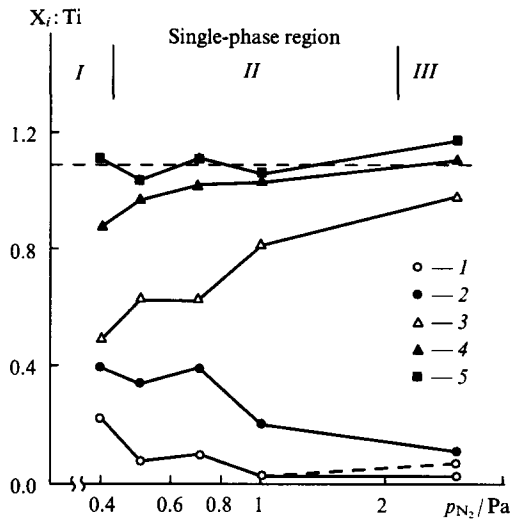


Figure 8. Dependence of the composition of the $Ti_xSi_yN_z(O)$ films on the nitrogen pressure. X: (*1*) Si; (*2*) O; (*3*) N; (*4*) O + N; (*5*) O + N + Si.

unexpected — it increases in parallel with increase in the oxygen content up to 0.3, which is much greater than the Si : Ti ratio in the target employed (~0.1).

It was established that, within the narrow range of nitrogen pressures $p_{N_2} = 6 \times 10^{-2} - 1 \times 10^{-1}$ Pa (region *II* in Fig. 8), the $TiSi_xN_yO_z$ films have a single-phase cubic structure. X-Ray photoelectron spectra indicate[110] identical energetics of the core states (Ti 2*p*, N 1*s*, O 1*s*) of these films and cubic titanium nitride and oxide nitride films.[53,54] The Si 2*p* silicon line is recorded distinctly in the region of the 99.1 eV binding energy. An estimate of the Si : Ti ratio based on XPES yielded ~0.04–0.12 depending on the film deposition conditions.[109,110] X-Ray probe microanalysis confirmed the presence of silicon and its uniform distribution in the cubic phase.

An increase in the lattice parameter of the siliconitride (from 4.16 to 4.28 Å) with increase in the silicon content was observed, which has been attributed to the differences between the atomic radii of silicon and nitrogen (1.71 and 0.71 Å respectively).[109]

The question of the sites occupied by the silicon atoms in the single-phase (of the NaCl type) $Ti_xSi_yN_z$ solid solutions, which was investigated by XPES, is of independent interest.[110] The binding energies of the Si 2*p*, Ti $2p_{3/2}$ N 1*s*, and O 1*s* core levels for a $TiSi_{0.1}N_{0.9}(O)$ film with a cubic structure and certain chemical compounds containing silicon and titanium are presented in Table 7. Evidently, in the specimens where silicon is the electron donor, oxygen or nitrogen atoms are disposed in its immediate environment and the maximum of the Si 2*p* level is displaced towards higher binding energies relative to the 'pure' silicon. On the other hand, if the first coordination sphere of silicon contains titanium atoms, the Si 2*p* line shifts towards lower binding energies.

Table 7. The binding energies (eV) for certain core levels in $Ti_xSi_yN_z(O)$ cubic (*B*1) films and certain titanium- and silicon-containing compounds according to X-ray photoelectron spectroscopy studies.

Compound	Ti $2p_{3/2}$	Si 2*p*	N 1*s*	O 1*s*
$Ti_5Si_3(O)$	454.1	98.8	–	530.9
$Ti_{0.7}Si_{0.25}O_{0.02}$ (target)	454.1	99.0	–	531.6
$Ti_xSi_yN_z(O)$	455.0	99.1	397.3	531.4
TiN(O)	455.1	–	397.3	531.5
Si	–	99.5	–	–
$Si_3N_4(O)$	–	101.7	397.5	531.3
SiO_2	–	103.1	–	532.4

The energy of the Si $2p$ level in the Ti–Si–N(O) film (99.1 eV) indicates the existence of a negative charge on the silicon atom and hence the disposition of these atoms in the nonmetallic sublattice of titanium oxynitrides.

A correlation between the content of silicon, nitrogen, and oxygen atoms and the degree of defectiveness has been observed[109,110] for all the $Ti_xSi_yN_z$ films investigated: in the region of the existence of the single-phase structure, the silicon content in the films increases simultaneously with increase in the oxygen concentration with retention of a virtually constant overall concentration of oxygen and nitrogen [(N + O)/ Ti ≈ 1.0]. The decrease in the quantity (N + O)/ Ti leads to an increase in the silicon concentration in the cubic $B1$ phase and one can therefore postulate that, as the degree of defectiveness of the nonmetallic sublattice and its oxygen content increase, the incorporation of silicon atoms into the $TiN(TiN_xO_y)$ structure becomes more favourable.

A synthesis of methastable cubic single-phase SS (as a coating) of the composition $Ti_{0.5}Si_{0.5}C$ by the magnetron sputtering method using a hot-pressed two-phase TiC / SiC target has been reported.[94] The preparation of single-phase SS based on TiC and including silicon was noted to be substantially more energy consuming (ion bombardment, heating of the substrate) than the preparation of aluminium-containing alloys like $Ti_{0.5}Al_{0.5}N$. This was attributed [94] to the lower mobility of atoms in the near-surface layer of TiC / SiC, which is due to the presence of strong covalent bonds. The localisation of the silicon atoms in the cubic structure of the $Ti_xSi_yC_z$ films has not been specially studied (it has been assumed implicitly that the silicon atoms substitute the metal atoms in TiC by analogy with the Al→Ti substitution). In our opinion, this problem needs to be further considered.

Simultaneously with the synthesis and the study of the structure and properties of films of the cubic $TiSi_xN_y$ phase, the computer simulation of the electronic characteristics of a series of cubic (of the NaCl type) alloys with a variable content of component atoms in the unit cell of the crystals was undertaken.[107,108] The relative stabilities of the hypothetical cubic solid solutions were investigated as a function of their composition and the possible mechanism of the substitution by silicon of different kinds of sites in the initial TiC and TiN matrices.

The following series of solid solutions were examined:

I. $TiC-TiSi_{0.25}C_{0.75}-TiSi_{0.50}C_{0.50}$; $TiN-TiSi_{0.25}N_{0.75}-TiSi_{0.50}N_{0.50}-TiSi_{0.75}N_{0.25}$.

II. $TiC-Ti_{0.75}Si_{0.25}C-Ti_{0.50}Si_{0.50}C$; $TiN-Ti_{0.75}Si_{0.25}N-Ti_{0.50}Si_{0.50}N$.

The process involving the formation of a solid solution on Si → (C,N) substitution was simulated for the series I solid solutions (by the LMTO method adopting TiC and TiN as the bases), whereas the substitution of silicon atoms by titanium atoms was simulated for the series II solutions.

Certain results of such simulation [107,108] are presented in Table 8 and in Fig. 9. Evidently, when silicon atoms are introduced into the bulk of the initial TiN, its spectrum is significantly transformed. On Si → N substitution, two intense DOS peaks arise near the upper and lower edges of the $p-d$ band and broaden markedly with increase in the silicon concentration, which diminishes the forbidden gap between the s and $p-d$ bands of TiN. A decrease in the intensity of the peak of the density of the N $2s$ states, as well as the partial emptying (as a consequence of the decrease in the concentration of valence electrons) of the antibonding (relative to the $p-d$ band) subband of the delocalised metallic states, a decrease in the density of states at the Fermi level $N(E_F)$, are observed at the same time.

On the other hand, on Ti → Si substitution the concentration of valence electrons in the cell does not change (9 e) and the Fermi energy does not actually shift; however, the perturbation of the TiN spectrum as a result of the introduction of the impurity is accompanied by an appreciable increase in $N(E_F)$.

A series of significant differences in the distribution of the LDOS of the elements comprising the solid solution have also been noted as a function of the type of sites occupied by silicon. These are caused primarily by the fundamentally different nature of the hybridisation of the valence states of silicon and the atoms coordinating it (SiN_6 or $SiTi_6$).[107] One may assume that fairly simple X-ray emission experiments (for example the study of the nitrogen and silicon K lines and the titanium L_α lines) may provide unambiguous evidence in support of one of the possible mechanisms of the incorporation of silicon in the crystal.

Table 8. The cohesion and substitution energies for solid solutions in the Ti–Si–C–N–O system.

Compound	$-E_{coh}$ / Ry	E_{sub} / Ry
TiN	1.32	–
$Ti_{0.75}Si_{0.25}N$	1.03	0.23
$Ti_{0.50}Si_{0.50}N$	0.72	0.53
$TiSi_{0.25}N_{0.75}$	1.13	0.18
$TiSi_{0.50}N_{0.50}$	1.05	0.21
$TiSi_{0.75}N_{0.25}$	1.01	0.25
$TiSi_{0.25}N_{0.50}$	0.92	0.37
$TiSi_{0.25}N_{0.50}O_{0.25}$	1.05	0.24
$TiSi_{0.25}N_{0.50}C_{0.25}$	1.21	0.08
TiC	1.59	–
$Ti_{0.75}Si_{0.25}C$	1.31	0.28
$Ti_{0.50}Si_{0.50}C$	1.05	1.54
$TiSi_{0.25}C_{0.75}$	1.42	0.17
$TiSi_{0.50}C_{0.50}$	1.28	0.31

The incorporation of silicon in TiC exerts an even greater influence on the electronic structure of the matrix (Fig. 9). In the completed state, the carbide may be classified as a semimetal.[1-4] Thus, whereas on substitution of silicon by carbon the Si $3p$ states are concentrated in the region of the $p-d$ subband and peak A corresponds to the atom-like nonbonding Si $3s$ resonance in the region of the forbidden gap between the C $2s$ and p subbands of the carbide (i.e. the bonding in $TiSi_xC_{1-x}$ is of the Ti $3d$–Si $3p$ hybrid type), in the $Ti_{1-x}Si_xC$ spectrum one can trace distinctly, apart from the additional Si $3s$-like maximum (in the vicinity of the lower edge of the C $2s$-type band) and the DOS peak (in the region of the forbidden gap of TiC of the mixed Si $3s$,$3p$ type), a progressive increase in the Si $3s$,$3p$ and C $2p$ local density of states (giving rise to the $p-p$ bonding) in the near-Fermi region of the crystal characterised by a deep DOS maximum for the ideal $TiC_{1.0}$.

The introduction of silicon at both N and Ti sites of the TiN lattice reduces appreciably the cohesion energy of the crystal, while the substitution energy is positive (Table 8). This should hinder the synthesis of homogeneous silicon-containing cubic solid solutions under equilibrium conditions, i.e. these solutions may be obtained predominantly in a metastable state.

On Si → N substitution (for solid solutions with identical silicon concentrations) $|E_{coh}|$ is greater and E_{sub} is smaller than the corresponding values calculated for the alloys where silicon is inserted at Ti sublattice sites (solid solutions containing identical silicon concentrations are compared), which indicates unambiguously that the substitution of nitrogen by silicon is preferable. With increase in the silicon concentration, $|E_{coh}|$ diminishes and there is a corresponding sharp increase in the positive E_{sub}, which indicates that the preparation of cubic solid solutions with a high silicon content becomes more difficult.

Comparison of the energy parameters of the silicon-containing nitride and carbide alloys shows [107,108] that the trends in the variation of E_{coh} and E_{sub} for the $Ti_xSi_yC_z$ solid solutions are the same as for titanium siliconitrides.

(1) The insertion of silicon at both Ti and C sites is an energetically unfavourable process, the Si → C substitution occurring more readily than Si → Ti.

(2) With increase in the silicon concentration, there is an appreciable decrease in $|E_{coh}|$ and an increase in E_{sub}, which is the

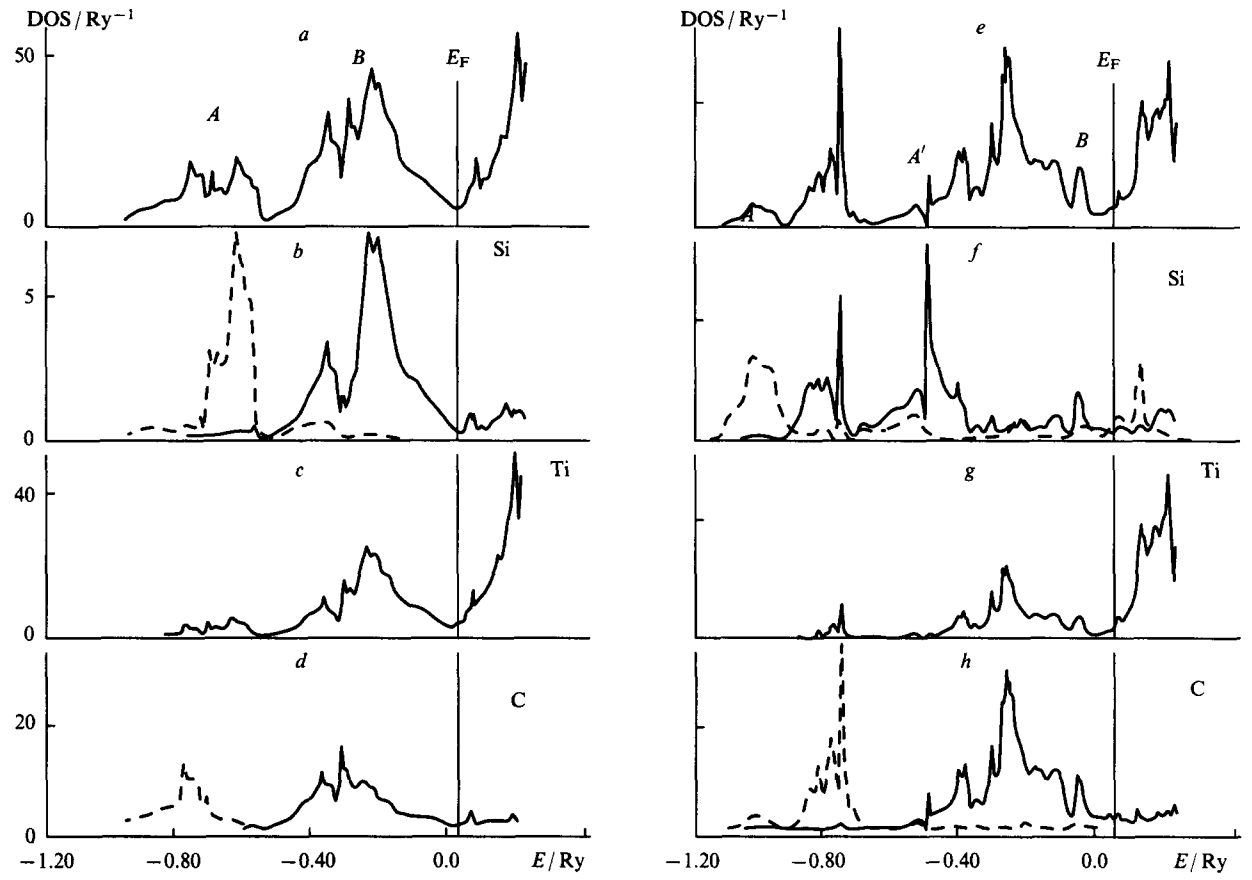


Figure 9. The total (*a*, *e*) and partial (*b*–*d*, *f*–*h*) DOS for the $TiSi_{0.25}C_{0.75}$ (*a*–*d*) and $Ti_{0.75}Si_{0.25}C$ (*e*–*h*) solid solutions.

reason for the instability of the silicon-enriched cubic solid solutions.

(3) In the Si → C substitution, silicon becomes involved in a *p*–*d* hybrid bond with the metal, whereas in the Si → Ti substitution the type of bond is determined by the mixing of the *p*–*p* functions.

The influence of impurities and N vacancies on the electron spectra and the stability of the cubic $TiSi_xN_y$ solid solution have been investigated within the framework of the LMTO method. The following compositions were examined:[108] $TiN_{1.0}$, $TiSi_{0.25}N_{0.75}$, $TiSi_{0.25}N_{0.50}$, and $TiSi_{0.25}N_{0.50}O_{0.25}$. In addition, the dependence of the equilibrium lattice parameter *R* of the $TiSi_xN_y$ alloys on the composition of the metalloid sublattice was determined.[108] Fig. 10 presents the dependence of the total energy of the alloys E_{tot} on *R*. Evidently, for the completed nitride $TiN_{1.0}$, the calculated parameter *R* = 4.22 Å agrees with the experimental value.[4,5] The incorporation of silicon atoms in the N sublattice leads to an appreciable increase in *R* (from 4.22 Å in $TiN_{1.0}$ to 4.32 Å in $TiSi_{0.25}N_{0.75}$). The presence of oxygen impurities or vacancies promotes a further increase in *R* (~4.34 Å for $TiSi_{0.25}N_{0.50}$ and $TiSi_{0.25}N_{0.50}O_{0.25}$), which agrees with experiment.[109,110]

Comparison of the DOS and LDOS distributions for the $TiN_{1.0}$, $TiSi_{0.25}N_{0.75}$, $TiSi_{0.25}N_{0.50}$, and $TiSi_{0.25}N_{0.50}O_{0.25}$ phases, obtained for equilibrium values of *R*, shows that the introduction of N defects is accompanied by a steady decrease in the contributions of the N 2*s*,2*p* states to the region of the occupied states of the spectrum and also by a significant redistribution of the valence states of titanium with the appearance of distinct *d* resonances, one of which is in the immediate vicinity and the other has the same energy as E_F (Fig. 11). The distribution of the 'vacancy' states is similar. The above features are due to the reorganisation of the states of the metallic centres coordinating the vacancy and reflect the partial 'elimination' of the splitting of the Ti states into bonding and antibonding. (This occurs for the completed TiX_6 immediate environment.) The Ti states pass to the region of nonbonding states (in the vicinity of E_F), giving rise to the 'vacancy' peaks in the DOS for titanium noted above. Some of the latter are 'trapped' by the sphere of the defect, giving rise to DOS vacancies.[9,10,102,108,111–114]

A different type of DOS distribution is observed for the $TiSi_{0.25}N_{0.50}O_{0.25}$ alloy (Fig. 11). The most notable changes in the electronic structures of the solid solutions, associated with the incorporation of oxygen atoms in their sublattices, consist[86,108] in the appearance of additional 'impurity' subbands of the O 2*s* and O 2*p* types, the former being of the quasi-core type and being located in the energy gap below the bottom of the valence band of

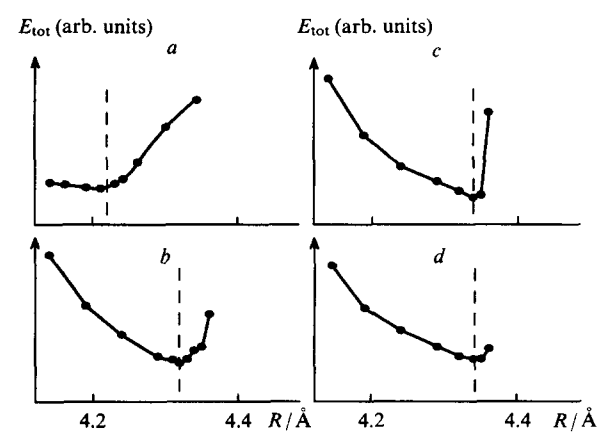


Figure 10. Dependence of the total energy of the crystal (E_{tot}) on the lattice constant for the $TiN_{1.0}$ (*a*), $TiSi_{0.25}N_{0.75}$ (*b*), $TiSi_{0.25}N_{0.50}$ (*c*), and $TiSi_{0.25}N_{0.50}O_{0.25}$ (*d*) cubic phases. Calculations by the LMTO method.

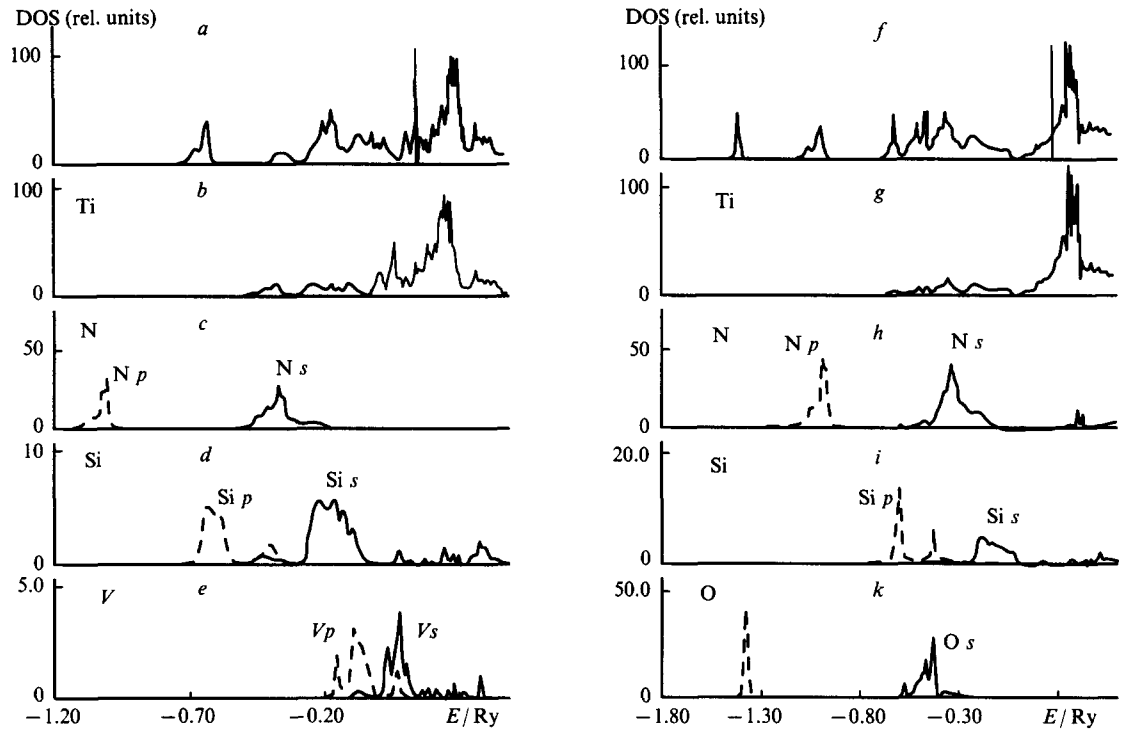


Figure 11. The energy distributions of the total (*a*, *f*) and partial (*b*–*d*, *g*–*k*) DOS for the nonstoichiometric (with respect to the N sublattice) $TiSi_{0.25}N_{0.50}$ (*a*–*c*) and $TiSi_{0.25}N_{0.50}O_{0.25}$ (*f*–*k*) cubic solid solutions. Calculation by the LMTO method. (*e*) Resolution of the 'vacancy' states into states with the *Vs* and *Vp* symmetries.

the siliconitride. The latter subband (of the O 2*p* type) is localised near the DOS minimum between Si 3s band and the hybrid *p*–*d* band of the matrix.

The influence of the defects considered on the energy state of the Ti–Si–N system has been discussed [86, 108] using the cohesion energies of the crystals and the substitution energies. It was established that the presence of the oxygen impurity or of lattice vacancies in the structure of the $TiSi_xN_y$ phase leads to a decrease in $|E_{coh}|$ and an increase in $|E_{sub}|$, indicating a progressive destabilisation of the system in the series $TiSi_{0.25}N_{0.75} \rightarrow TiSi_{0.25}N_{0.50}O_{0.25} \rightarrow TiSi_{0.25}N_{0.50}$. These data indicate a greater energy stability of the siliconitride with an oxygen impurity compared with the solid solution containing N vacancies.[109, 110]

The results of studies on the electronic properties of silicon-containing solid solutions retaining the basic structure of the initial binary phases — sphalerite (SiC) or rock salt (TiC, TiN) — have been considered hitherto.

The study of the phase equilibria in the Ti–Si–C system made it possible to establish the existence of at least two ordered silicocarbide phases — $Ti_5Si_3C_x$ and Ti_3SiC_2.[1–3, 88, 92, 115–117] Among these phases, the Ti_3SiC_2 phase with a hexagonal structure ($P6_3/mmc$ space group, unit cell parameters a = 3.066 Å, and c = 17.646 Å), in which the metal atoms occupy two structurally nonequivalent sites with and without silicon atoms in their immediate environment (Fig. 12), has attracted the greatest attention recently.[93, 94, 116, 117] It plays a significant role in the formation of the microstructure of the contact band of ceramics of the type TiC / SiC and Ti / SiC.[92–94] The development of ceramic polycrystalline materials based on titanium silicocarbide has been reported.[88–93]

The band structure of Ti_3SiC_2 has been calculated by the full-potential self-consistent LMTO method.[118]

In contrast to the electron structure of the binary titanium carbide,[7–10] E_F for the electronic structure of the silicocarbide coincides with the peak of the density of the *d* states of titanium (Fig. 13), which should give rise to the metal-like properties of this phase. The contributions to $N(E_F)$ by the states of the structurally nonequivalent titanium atoms are significantly different, the Ti(1) states playing a decisive role $[N(E_F)_{Ti(1)} : N(E_F)_{Ti(2)} \approx 3.76]$.

The form and energy distribution of the DOS for the Ti(1) and Ti(2) atoms are also different (Fig. 13). Thus, whereas the DOS for the Ti(1) atoms, having both Si and C centres in its environment, contains two maxima with energies identical with those of the DOS peaks for carbon and silicon, the valence states of the Ti(2) atoms, containing only carbon atoms in the first coordination sphere, are displaced downwards on the energy scale [relative to the density of states of the Ti(1) type], whereas the form of the density of states for the Ti(2) centres repeats in many respects the form of the C 2*p* states.

An estimate of the effective charges on the atoms [+ 0.614 e for Ti(1); + 0.641 e for Ti(2); −0.304 e for Si; −0.384 e for C] indicates partial charge transfers in the Ti(1,2) → Si direction, which ensures the existence of an ionic component in the overall chemical bonding system in Ti_3SiC_2. Consequently a combined ionic-covalent-metallic type of chemical bonding arises in Ti_3SiC_2. It is determined by the charge polarisation between the

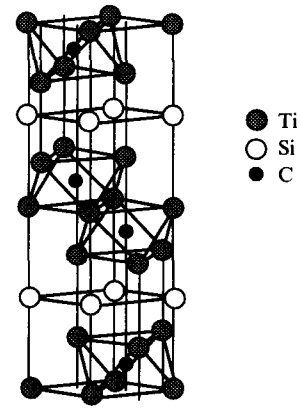


Figure 12. A fragment of the Ti_3SiC_2 crystal structure.

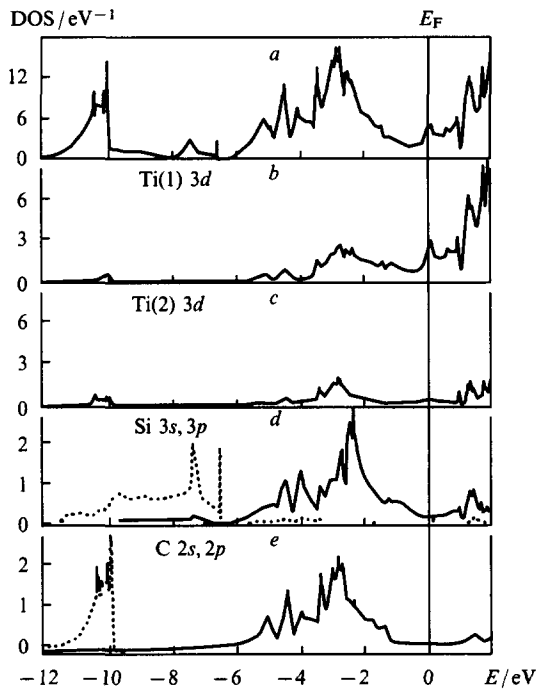


Figure 13. The total (*a*) and partial (*b*–*e*) DOS for Ti_3SiC_2. For the significance of Ti(1) and Ti(2), see text.

atoms of the metal and the metalloids, the hybridisation of the valence states [of the Ti(1) 3*d*–Si 3*p*, Ti(1) 3*d*–C 2*p*, Ti(2) 3*d*–C 2*p*, and Si 3*p*–Si 3*p* types], and the delocalisation of the near-Fermi *d* states of titanium [mainly of the Ti(1) atoms].[118]

The next stage in the study of the electronic properties of titanium silicocarbides (as well as the silicocarbides of other transition metals) should include a more detailed description of the chemical bonding, its anisotropy, and its influence on the properties of the silicon-containing phases.

IV. Chemical bonding in ternary carbides and nitrides based on subgroup VIIA and VIIIA transition metals

The compounds based on subgroup VIIA and VIIIA transition metals constitute a representative class of ternary carbides and nitrides.[1–3,29–32] The carbides $M_3M'C$ (M is a transition metal and M′ are subgroup IIIB and IVB nontransition elements) have been most thoroughly investigated. The magnetic characteristics of these compounds as well as the magnetic and structural phase transitions, observed in the temperature range 200–500 K, have attracted the greatest attention of investigators.[29–32] In the high-temperature region, these compounds have a cubic structure of the antiperovskite type[1–3,119–128] and are paramagnetic materials of the Pauli type; at lower temperatures, tetragonal lattice distortions as well as second-order magnetic phase transitions with formation of several possible types of ordered magnetic structures have been discovered for the series of carbides.[29–32,129–142]

The first model of the interatomic interactions and the electronic states in the $M_3M'C$ phases was proposed by Jardin and Labbe.[143–145] According to this model, the carbides have an extended conductivity band, which overlaps with a narrow band of hybrid states made up of contributions by the M *d* and C 2*p* orbitals. The distribution of the DOS for this band has been estimated with the aid of the approximate tight-binding scheme.[145] A logarithmic singularity has been observed in the DDS near its energy centre. Postulating that the Fermi level E_F is located near the peak of the antibonding *p*–*d* subband, Jardin and Labbe[143–145] explained the instability of the crystal and magnetic structures of $M_3M'C$ on the basis of the characteristics of the electronic structure which they postulated.

We may note that this model was not confirmed in subsequent numerical calculations for the series of perovskite-like carbides.

The first self-consistent LAPW calculations for $Mn_3M'C$ (M′ = Zn, Ga, In, Sn) in a nonmagnetic high-temperature state (cubic structure) established[146,147] that the near-Fermi region of the carbide is made up mainly of the *d* states of the transition metal, whereas the valence bonding (antibonding) subbands for the other component atoms are located somewhat below (above) the Fermi level. Estimates of the local magnetic moments (LMM), carried out with the aid of spin-polarised calculations for the ferromagnetic states of Mn_3GaC, showed[146] that the Mn 3*d* states undergo the maximum spin splitting; the LMM on the atoms are 1.35 μ_B (Mn), −0.12 μ_B (C), and −0.008 μ_B (Ga), the estimates being quite reasonably correlated with experiment (the LMM on Mn is 1.3 ± 0.1 μ_B at 193 K).[32]

Systematic LMTO calculations for the cubic carbides $M_3M'C$ (M = Mn, Fe; M′ = Zn, Al, Sn, Ga) made it possible to discover[148,149] the rules governing the variation of the electronic structures of the compounds as a function of the composition of the M and M′ lattices. Fig. 14 presents as an example the electronic states of Mn_3ZnC. Evidently the valence band contains four distinct subbands. The lower subband is of the quasi-core type and is made up mainly of the contributions of the C 2*s* states with slight additional contributions of the Zn 3*d*, Mn 3*d*, and Zn 4*s* states. The next bonding band includes the hybrid C 2*p*–Mn 3*d* functions as well as the pseudoatomic resonances of the Zn 3*d* and Zn 4*s* states. The nonbonding, partly filled near-Fermi subband is determined by the dispersion of the Mn 3*d*

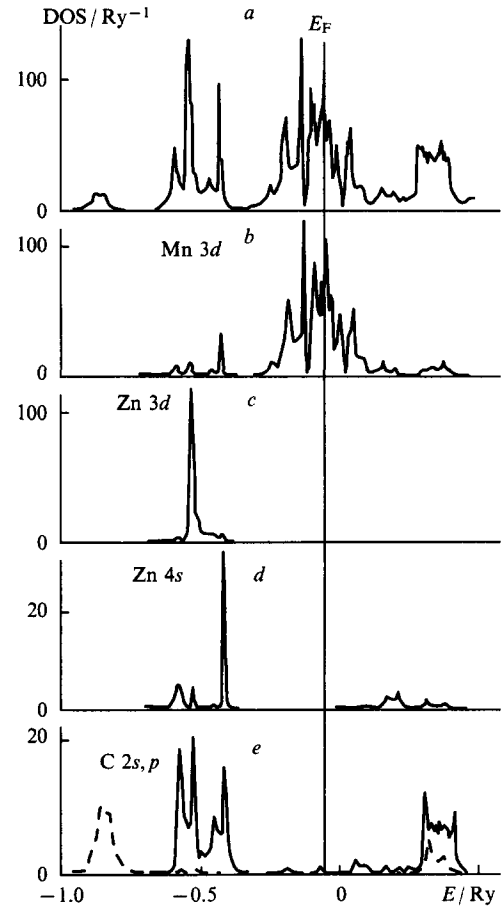


Figure 14. The total (*a*) and partial (*b*–*e*) DOS for the nonmagnetic Mn_3ZnC. Calculations by the LMTO method.

Table 9. The partial charges in the atomic spheres (q / e) and the differences between the charges in the atomic spheres in the crystal and in the free state (Δq / e) in manganese and iron carbides.

Charge	Mn_3ZnC	Mn_3AlC	Mn_3SnC	Mn_3GaC	Charge	Fe_3ZnC	Fe_3AlC	Fe_3SnC
q(Mn,s)	1.616	1.670	1.645	1.598	q(Fe,s)	1.682	1.704	1.698
q(Mn,p)	1.844	1.974	2.065	1.916	q(Fe,p)	1.856	1.964	2.058
q(Mn,d)	3.207	3.153	3.175	3.218	q(Fe,d)	4.207	4.158	4.178
Δq(Mn)	+0.333	+0.221	+0.115	+0.268	Δq(Fe)	+0.255	+0.174	+0.066
q(M′,s)[a]	1.122	1.238	1.480	1.472	q(M′,s)	1.060	1.242	1.500
q(M′,p)	0.650	1.392	1.973	1.521	q(M′,p)	0.928	1.280	1.848
q(M′,d)	10.030	0.226	0.	0.	q(M′,d)	9.886	0.226	0.0
Δq(M′)	+0.198	+0.144	+0.547	+0.007	Δq(M′)	+0.126	+0.252	+0.652
q(C,s)	1.426	1.420	1.396	1.428	q(C,s)	1.430	1.424	1.382
q(C,p)	3.374	3.388	3.494	3.384	q(C,p)	3.458	3.348	3.466
Δq(C)	−0.800	−0.808	−0.890	−0.812	Δq(C)	−0.888	−0.772	−0.848

[a] M′ = Zn, Al, Sn, or Ga.

states, with a lower vacant antibonding band including the C 2p and Mn 3d states. The above four-band structure is characteristic of all the carbides examined [146–149] and the changes in the composition of the M′ sublattice influence only the energetics of the 'centre of gravity' of the M′ subband and the degree of their splitting (into bonding and antibonding components). Furthermore, the change in the concentration of valence electrons on replacement of the nontransition metal by elements of a different kind determines the position of E_F relative to the near-Fermi resonance of the M 3d type. Thus the Fermi level for Mn_3SnC coincides with the DOS peak, as a result of which $N(E_F)$ is a maximum in the above series of compounds. This can be treated as the factor responsible for the minimal stability of the cubic structure of the given carbide, which undergoes lattice distortions or variations in composition.[1,2,119–122]

The Mn → Fe replacement in the above phase leads (as a consequence of the decrease in the lattice parameter) to a somewhat greater splitting of the bonding and antibonding sub-bands [148,149] and also to the filling of the nonbonding states, whereupon $N(E_F)$ reaches a maximum value for Fe_3AlC.

As regards the nature of the interatomic interactions, analysis shows [148,149] that, apart from the direct bonds linking transition and nontransition metals to one another and covalent M–C interactions of the p–d type, the chemical bonding system in crystals is supplemented by interactions of the s–s, s–p, and p–p types between nontransition metals and carbon. In addition, it follows from Table 9 that partial transfer of charge density from metals (transition and nontransition) to the sphere of the carbon atom is observed, but in the case of compounds with the same M′ sublattice [for example, $Mn_3M'C$ and $Fe_3M'C$ (Table 9)] the effective positive charges are found to be higher for manganese than for iron. We may note that in this respect the situation repeats the familiar tendency in binary carbides, where the ionic component of the bond diminishes with increase in the atomic number of the carbide-forming metal.[7–12]

The band structures and magnetic properties of individual representatives of the carbides $M_3M'C$, in the first place the relative stabilities of the possible types of ordering of the spin subsystem, have been investigated.[150–153]

The total energy has been estimated by the LAPW method for the nonmagnetic, ferromagnetic, and antiferromagnetic states of Mn_3GaC as a function of the volume of the unit cell.[150] It was established that the ferromagnetic spin ordering is energetically most preferred for the equilibrium volume, since with increase in the lattice constant a transition from the ferromagnetic to the antiferromagnetic state (FM → AFM) should be observed. This finding conflicts with experiments [153,154] according to which the AFM state is established at $T < 165$ K. The authors [150] attribute this discrepancy to the use of the spherically-symmetrical approximation to the potential.

An attempt to take into account the influence of the tetragonal lattice distortion on the photoelectron spectra of the $Mn_3M'C$ (M′ = In, Sn) has been undertaken [151] within the framework of the LMTO ASA method wherein the manganese atoms are at two structurally nonequivalent sites [Mn(I) and Mn(II)], which is significantly reflected both in the distribution of their DOS (Fig. 15) and in the local magnetic moments localised on the given atoms, the difference between which amounts to ~1.59 μ_B for Mn_3SnC (in the ferromagnetic state) and to ~1.17 μ_B for Mn_3InC. Together with the ferromagnetic spin ordering, ferrimagnetic spin ordering as well as the possibility of their coexistence were investigated. An estimate of the total energy for the above cases made it possible to claim [151] that a 'mixed' state of the spin subsystem is most probable.

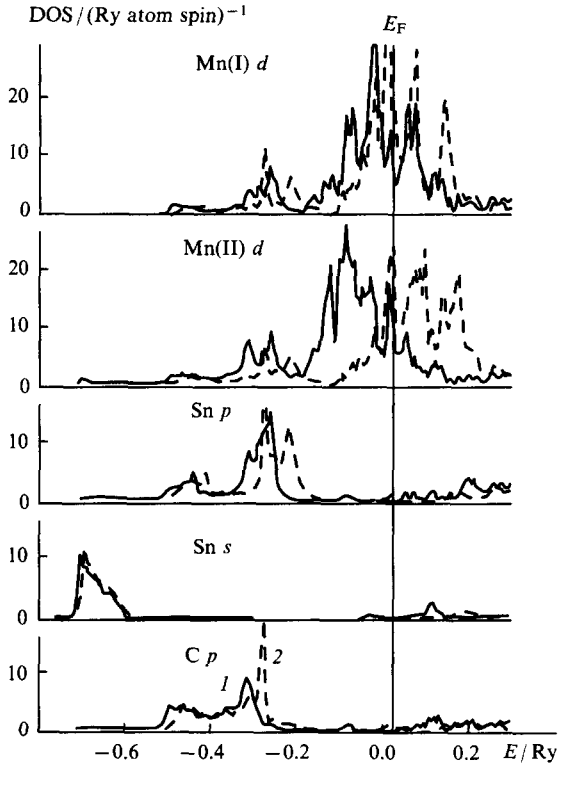


Figure 15. The partial DOS for the Mn_3SnC ferromagnetic phase with a tetragonal structure. The DOS for the structurally nonequivalent manganese atoms [Mn(I) and Mn(II)] with 'upward' (*1*) and 'downward' (*2*) spin directions. Calculation by the LMTO method.

The type of transition (FM ⇄ AFM) has been determined [151] in relation to Mn_3GaX (X = C, N) as a function of the composition of the metalloid sublattice and the lattice constant (the LMTO ASA method). In contrast to the preceding data,[151] it was established that, for the equilibrium value of the lattice constant, the AFM state is the most stable for Mn_3GaC, the maximum local magnetic moment corresponding to it (the local magnetic moment on the manganese atom is 1.63 μ_B for AFM and 1.39 μ_B for FM); the local magnetic moment increases with increase in the lattice constant. The local magnetic moment on the manganese atom in Mn_3GaN is 1.52 μ_B,[152] which exceeds somewhat the experimental value of 1.17 μ_B.[32]

In contrast to carbides, the available information about the electronic properties of the ternary nitrides belonging to the class under discussion is extremely limited. With the exception of the study already mentioned,[152] we are aware only of calculations for the nitride Fe_3SnN [155] and also for Fe_3MnN and Fe_3PdN,[156] carried out by the LMTO method. The main task of the above investigations [155,156] was to determine the influence of partial substitution of the iron atoms in the face-centred cubic crystal structure of γ-Fe_4N by elements of a different kind on the parameters of the band structure and on the stability and magnetic properties of the latter.

The magnetic characteristics of the cubic Fe_4N have now been investigated in fair detail both experimentally [157-159] and theoretically (by the quantum-chemical computational method).[160-162]

In the series of ternary nitrides listed above, the electronic structure of the Fe_3SnN alloy is of greatest interest in the context of this review.[155] According to Mössbauer spectroscopic data,[158,163] the tin atoms are inserted predominantly at the sites occupied by the Fe(1) atoms located at the vertices of the γ-Fe_4N unit cell [in contrast to the Fe(2) atoms, which are at the centres of its lateral faces].

In order to take into account the influence of the size factor [in the Sn → Fe(1) substitution], calculations were made of the DOS with the lattice constant varied in the range ~7.17–7.46 a.u. It was established [155] that the energy bands close to E_F are made up mainly of the Fe *d* states, which make the maximum contribution to $N(E_F)$, with only slight additional contributions by the Sn *d* and N *p* states. The introduction of the tin impurity into the perovskite-like γ-Fe_4N diminishes appreciably the overall magnetisation of the system from 9.40 to 6.00 μ_B (per formula unit) respectively. The contributions of iron to $N(E_F)$ and the local magnetic moments on the given centres in Fe_3SnN exceed in their turn the corresponding values for Fe(2) in γ-Fe_4N.

The dependence of the local magnetic moments on the Fe(1) and Fe(2) atoms in γ-Fe_4N and on the iron atoms in Fe_3SnN on the lattice parameter is extremely interesting (Fig. 16). It shows that the 'contraction' of the crystals (by 10% of the volume) has the most 'dramatic' effect on the local magnetic moments on the Fe(2) and Fe centres: as a result of the contraction, they diminish sharply up to the disappearance of the local magnetism on the Fe(2) atoms of the γ-nitride. A similar phenomenon had been observed earlier for iron [164-167] in a series of Fe–Pd and Fe–Ni invar alloys with a face-centred cubic structure.[168] The above 'magnetic collapse' effect on decrease in volume can be accounted for by the appearance of several magnetic phases. The wide scale employment of this model for the interpretation of the nature of the variation of the local magnetic moments on the Fe centres of the nitrides requires correct calculations of the total energies of these objects for different types of spin ordering.

Finally, the results of Kuhnen and dos Santos [155] make it possible to describe the charge transport and the nature of the interatomic bonds in Fe_3SnN. The effective atomic charges [−1.415 e (Sn), + 0.658 e (Fe), and − 0.560 e (N)] indicate the transfer of charge density into the sphere of the iron atoms. As regards the nature of the chemical bonding, analysis of the form of the LDOS for the component atoms permits the conclusion that the nitrogen atoms are mainly involved in covalent *p*–*d* bonds with the iron atoms to which they are coordinated, the outer states

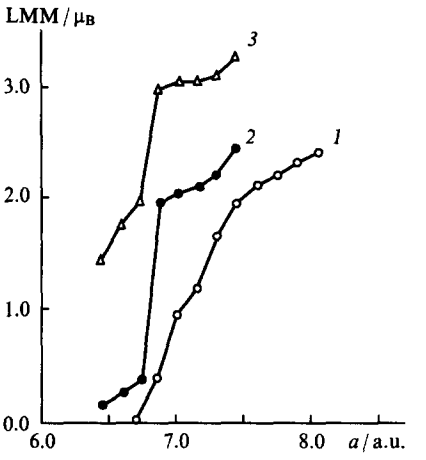


Figure 16. Dependence of the local magnetic moments of iron [Fe(1) and Fe(2), see text] for γ-Fe_4N and of the iron atoms in Fe_3SnN on the lattice parameter: (*1*) Fe; (*2*) Fe(2); (*3*) Fe(1).

of the latter becoming mixed with the *s*,*p* functions of the Sn centres and the *s*,*p*,*d* states of the neighbouring (in the Fe_6N octahedron) iron atoms, whereas the Sn–N interaction is assumed [155] to be negligible. Finally, the determination of the types of interatomic interactions, predominating in the organisation of the overall chemical bonding system in the crystal and responsible for its structural and physicochemical properties, requires more detailed calculations, including the estimation of pair (and multicentre) bonds of different nature as regards energy.

* * *

In conclusion we may note that, despite the fact that the studies on the electronic properties of complex carbides and nitrides of transition metals and subgroup IIIB and IVB elements began fairly recently, the results obtained hitherto constitute a fairly promising basis for a correct interpretation of the fundamental features of the electronic structure, the nature of the chemical bonding, the charge distributions, and certain properties (in the first place spectroscopic and magnetic) of the groups of the above substances which are of greatest interest and practical significance.

Priorities in further research are formulated taking into account the results obtained. Among such priorities, one may include the determination of the characteristics of the transformation of the properties of ideal three-component systems under the influence of impurities, defects (in the ordered and disordered states), and crystal distortions as well as under the influence of their combined action. The mechanical, thermal, strength, and catalytic properties, which determine the technological aspects of the employment of the phases under discussion, have been virtually uninvestigated (from the theoretical standpoint). The development of models and numerical calculations of the above properties (which may also be predictive in nature) should constitute the next stage in the study of such phases. Investigations designed to achieve a theoretical description and modelling of the heterophase (in the structural and magnetic respects) materials based on the substances considered will be of undoubted importance.

References

1. H J Goldschmidt *Interstitial Alloys* (London: Butterworths, 1967)
2. G V Samsonov, G Sh Upadkhaya, V S Neshpor *Fizicheskoe Materialovedenie Karbidov* (Physical Materials Science of Carbides) (Kiev: Naukova Dumka, 1974)
3. L E Toth *Transition Metal Carbides and Nitrides* (New York: Academic Press, 1971)

4. G V Samsonov, I M Vinitskii *Tugoplavkie Soedineniya* (High-Melting Compounds) (Moscow: Mir, 1976)
5. G V Samsonov, O P Kulik, V S Polishchuk *Poluchenie i Metody Analiza Nitridov* (Synthesis and Methods of Analysis of Nitrides) (Kiev: Naukova Dumka, 1978)
6. T Ya Kosolapova (Ed.) *Svoistva, Poluchenie i Primenenie Tugoplavkikh Soedinenii. Spravochnik* (Properties, Synthesis, and Application of High-Melting Compounds. Handbook) (Moscow: Metallurgiya, 1986)
7. J Calais *Adv. Phys.* **26** 847 (1977)
8. A Neckel *Int. J. Quantum Chem.* **23** 1317 (1983)
9. A L Ivanovskii, V A Gubanov, G P Shveikin, E Z Kurmaev *Usp. Khim.* **52** 705 (1983) [*Russ. Chem. Rev.* **52** 395 (1983)]
10. A L Ivanovskii, V P Zhukov, V A Gubanov *Elektronnoe Stroenie Tugoplavkikh Karbidov i Nitridov Perekhodnykh Metallov* (Electronic Structure of Refractory Carbides and Nitrides of Transition Metals) (Moscow: Nauka, 1990)
11. R Freer (Ed.) *The Physics and Chemistry of Carbides, Nitrides, and Borides* (Dordrecht: Kluwer, 1990)
12. A L Ivanovsky, G P Shveikin *Phys. Status Solidi B* **181** 251 (1994)
13. G V Samsonov *Nemetallicheskie Nitridy* (Nonmetallic Nitrides) (Moscow: Metallurgiya, 1969)
14. T Lundstrom, S Rundqvist (Eds) *Borides, Silicides, and Phosphides* (London: Methuen, 1965)
15. T Ya Kosolapova, T V Andreeva, T B Bartnitskaya, G G Gnesin, G N Makarenko, I I Osipova, E V Prilutskii *Nemetallicheskie Tugoplavkie Soedineniya* (Nonmetallic High-Melting Compounds) (Moscow: Metallurgiya, 1985)
16. J Kallwait *Theory of Energy Band Structure* (Translated into Russian; Moscow: Mir, 1969)
17. W A Harrison *Electronic Structure and the Properties of Solids* (Translated into Russian; Moscow: Mir, 1983)
18. E A Zhurakovskii, I N Frantsevich *Rentgenovskie Spektry i Elektronnaya Struktura Silitsidov i Germanidov* (X-Ray Spectra and Electronic Structure of Silicides and Germanides) (Kiev: Naukova Dumka, 1981)
19. V V Sobolev, V V Nemoshkalenko *Metody Vychislitel'noi Fiziki v Teorii Tverdogo Tela. Elektronnaya Struktura Poluprovodnikov* (Methods of Computational Physics in the Theory of Solids. Electronic Structure of Semiconductors) (Kiev: Naukova Dumka, 1988)
20. A Katz (Ed.) *Indium Phosphide and Related Materials: Processing, Technology, and Devices* (Boston: Artech House, 1992)
21. S Adachi *Physical Properties of III-V Semiconductor Compounds: InP, InAs, GaAs, InGaAs, and InGaAsP* (New York: Wiley, 1992)
22. J E Sundgren, B O Johansson, S E Carlsson *Thin Solid Films* **105** 353 (1983)
23. O Knotec, T Leyendecker *J. Vac. Sci. Technol.* **5** 2173 (1986)
24. O Knotec, T Leyendecker *J. Solid State Chem.* **70** 318 (1987)
25. L Hultman, G Hakansson, U Wahlstrom, J Sundgren *Thin Solid Films* **205** 133 (1991)
26. R Strydom, S Hoffman *J. Electron Spectrosc. Relat. Phenom.* **56** 85 (1991)
27. P J Martin *Thin Solid Films* **153** 91 (1987)
28. K Upadhya *JOM* (5) 15 (1992)
29. Le Dang Khoi, E Fruchart, D Fruchart *Solid State Commun.* **8** 49 (1970)
30. D Fruchart, E F Bertaut, F Sayetat, G Lorthioir, R Madar, A Ronault *Solid State Commun.* **8** 91 (1970)
31. A Kenmotsu, T Shinohara, H Watanabe *J. Phys. Soc. Jpn.* **32** 377 (1972)
32. D Fruchart, E F Bertaut *J. Phys. Soc. Jpn.* **44** 781 (1978)
33. G Hakansson, J E Sundgren *Thin Solid Films* **153** 55 (1987)
34. M V Kuznetsov, S V Borisov, Yu F Zhuravlev, R S Baryshev, O F Denisov, B V Mitrofanov, V A Gubanov *Poverkhnost'* (12) 141 (1989)
35. M V Kuznetsov, E V Shalaeva, V A Gubanov *Poverkhnost'* (2) 95 (1994)
36. D T Quinto *Thin Solid Films* **153** 37 (1987)
37. A J Herman, S Hoffman *Thin Solid Films* **153** 45 (1987)
38. R Luthier, F Levy *J. Vac. Sci. Technol. A, Vac. Surf. Films* **9** 102 (1991)
39. S Inomura, K Nobugai, F Kanamura *J. Solid State Chem.* **68** 124 (1987)
40. H A Jehn, S Hoffmann, V E Ruckborn, D W Munz *J. Vac. Sci. Technol. A, Vac. Surf. Films* **4** 2701 (1986)
41. O Knotek, M Boehmer, T Leyendecker *J. Vac. Sci. Technol. A, Vac. Surf. Films* **4** 2695 (1986)
42. H Freller, H Haessler *Thin Solid Films* **153** 67 (1987)
43. D W Muenz *J. Vac. Sci. Technol. A, Vac. Surf. Films* **4** 2717 (1987)
44. G Hakansson, J E Sundgren, D McIntyre, J E Greene, D W Munz *Thin Solid Films* **153** 55 (1987)
45. D McIntyre, J E Greene, G Hakansson, J E Sundgren, D W Munz *J. Appl. Phys.* 67 1542 (1990)
46. I Pentinnen, J M Molatius, A S Korhonen, R Lappalainen *J. Vac. Sci. Technol. A, Vac. Surf. Films* **6** 2158 (1988)
47. D Zlatanovic, P Stosic *Vacuum* **39** 557 (1989)
48. H Randhawa, P C Johnson, R Cunningham *J. Vac. Sci. Technol. A, Vac. Surf. Films* **6** 2136 (1988)
49. A M Dorodnov, V A Potrosov *Zh. Tekh. Fiz.* **51** 504 (1981)
50. G Lemperiere, J M Poltivin *Thin Solid Films* **111** 353 (1984)
51. M V Kuznetsov, J F Zhuravlev, E V Shalaeva *Thin Solid Films* **215** 1 (1992)
52. M V Kuznetsov, Yu F Zhuravlev, V A Gubanov *Zashch. Met.* 28 (1992)
53. M V Kuznetsov, Yu F Zhuravlev, D L Novikov, V A Gubanov *Poverkhnost'* (1) 131 (1990)
54. M V Kuznetsov, Candidate Thesis in Physicomathematical Sciences, Institute of Chemistry, Ural Branch of the Academy of Sciences of the USSR, Sverdlovsk, 1989
55. D Briggs, M P Seakh *Practical Surface Analysis by Auger and X-Ray Photoelectron Spectroscopy* (New York: Wiley, 1983)
56. U Gelius *Electron Spectroscopy* (Amsterdam: North-Holland, 1972)
57. H Hochst, R D Bringans, P Steiner, T Wolf *Phys. Rev. B, Condens. Matter* **25** 7183 (1982)
58. L Porte, L Roux, J Hanus *Phys. Rev. B, Condens. Matter* **28** 3214 (1983)
59. R D Bringans, H Hochst *Phys. Rev. B, Condens. Matter* **30** 5416 (1984)
60. H Nowotny, P Ettmayer *J. Inst. Met.* **97** 180 (1969)
61. V I Ivchenko, M I Lesnaya, V F Nemchenko, T Ya Kosolapova *Poroshk. Metall.* (5) 45 (1976)
62. I A Brytov, V S Neshpor, Yu N Romashchenko, E A Ivchenko *Fiz. Met. Metalloved.* **56** 253 (1983)
63. A L Ivanovskii, Doctoral Thesis in Chemical Sciences, Institute of Chemistry, Ural Scientific Centre of the Academy of Sciences of the USSR, Sverdlovsk, 1988
64. A L Ivanovskii, I V Solov'ev, V A Gubanov *Zh. Neorg. Khim.* **32** 1754 (1987)
65. A L Ivanovskii, V I Anisimov, I V Solov'ev, V A Gubanov *Izv. Akad. Nauk SSSR. Neorg. Mater.* **24** 1311 (1988)
66. A L Ivanovsky, R F Sabiryanov *J. Phys. Chem. Solids* **54** 1061 (1993)
67. D E Ellis, G S Painter *Phys. Rev. B, Condens. Matter* **9** 2887 (1970)
68. V A Gubanov, A L Ivanovsky, G P Shveikin, D E Ellis *J. Phys. Chem. Solids* **45** 719 (1984)
69. J Petru, J Klima, P Herzig *Z. Phys. B, Condens. Matter* **76** 483 (1989)
70. D Vogtenhuber-Pawelczak, P Herzig, J Klima *Z. Phys. B, Condens. Matter* **84** 211 (1991)
71. P Herzig, J Redinger, R Eibler, A Neckel *J. Solid State Chem.* **70** 281 (1987)
72. J Redinger, R Eibler, P Herzig, A Neckel, R Podloucky, E Wimmer *J. Phys. Chem. Solids* **47** 387 (1986)
73. A Neckel *Int. J. Quantum Chem.* **23** 1317 (1983)
74. A Neckel, K Schwarz, R Eibler, P Weinberger *Ber. Bunsenges. Phys. Chem.* **79** 1053 (1975)
75. L Szunyogh, J Klima, D Vogtenhuber-Pawelczak, P Herzig, P Weinberger *Z. Phys. B, Condens. Matter* **85** 281 (1991)
76. B Gyorffy, M J Stott, in *Band Structure Spectroscopy of Metals and Alloys* (Eds F J Fabian, L M Watson) (New York: Academic Press, 1968) p. 385
77. P Weinberger *Electron Scattering Theory for Ordered and Disordered Matter* (Oxford: Clarendon Press, 1990)
78. E Beaupres, C F Hagne, J M Mariot, P Weinberger *Phys. Rev. B, Condens. Matter* **34** 886 (1986)
79. G Wiech, E Zoepf *J. Phys. (France)* **32** C4-200 (1971)
80. J Redinger, P Marksteiner, P Weinberger *Z. Phys. B, Condens. Matter* **63** 321 (1986)
81. H Winter, P I Durham, G M Stocks *J. Phys. F, Met. Phys.* **14** 1047 (1984)
82. G Hoermandinger, P Weinberger, P Marksteiner, J Redinger *Phys. Rev. B, Condens. Matter* **38** 1040 (1988)

83. G Hoermandinger, P Weinberger, J Redinger *Phys. Rev. B, Condens. Matter* **40** 7989 (1989)
84. A L Ivanovsky, N I Medvedeva, G P Shveikin *Mendeleev Commun.* 176 (1994)
85. N I Medvedeva, A L Ivanovskii *Zh. Neorg. Khim.* **40** 1195 (1995)
86. A L Ivanovsky, N I Medvedeva, G P Shveikin, V M Zhukovsky *Phys. Status Solidi* (1996) (in the press)
87. H L Skriver *The LMTO Method* (London: Springer, 1984)
88. J J Nickl, K K Schweitzer *Z. Met.kd.* **6** 54 (1970)
89. J Lis, R Pampuch, J Piekarczyk, L Stobierski *Ceram. Int.* **19** 219 (1993)
90. B Gottselig, E Gyarmati, A Naoumidis, H Nickel *J. Eur. Ceram. Soc.* **6** 153 (1990)
91. J Lis, R Pampuch, L Stobierski *Int. J. Self-Propag. High-Temp. Synth.* **1** 401 (1992)
92. R Pampuch, J Lis, L Stobierski, M Tymkiewicz *J. Eur. Ceram. Soc.* **5** 283 (1989)
93. H Holleck *Surf. Coat. Technol.* **36** 151 (1988)
94. R Fella, H Holleck *Mater. Sci. Eng.* **A140** 676 (1991)
95. R F Sabiryanov, A L Ivanovskii, G P Shveikin *Zh. Neorg. Khim.* **38** 1572 (1993)
96. F Herman, J P van Dyke, R L Kortum *Mater. Res. Bull.* **14** 167 (1969)
97. F Bassani, M Yashimine *Phys. Rev.* **130** 20 (1964)
98. L A Hemstreet, C Y Fong *Solid State Commun.* **9** 643 (1971)
99. A R Lubinsky, D E Ellis, G S Painter *Phys. Rev. B, Condens. Matter* **11** 1537 (1975)
100. K J Chang, M L Cohen *Phys. Rev. B, Condens. Matter* **35** 8196 (1987)
101. M Causa, R Dovesi, C Roetti *Phys. Rev. B, Condens. Matter* **43** 937 (1991)
102. V I Anisimov, V P Antropov, V A Gubanov, A L Ivanovskii, A V Postnikov, E Z Kurmaev *Elektronnaya Struktura Defektov i Primesei v Metallakh, Splavakh i Soedineniyakh* (Electronic Structure of Defects and Impurity in Metals, Alloys, and Compounds) (Moscow: Nauka, 1989)
103. Zh V Gertner, N I Medvedeva, V M Zhukovskii, A L Ivanovskii, G P Shveikin *Metallofiz. Noveishie Tekhnol.* **16** 78 (1994)
104. N I Medvedeva, Zh V Gertner, V V Kraskovskaya, A L Ivanovskii, G P Shveikin *Neorg. Mater.* **31** 55 (1995)
105. V P Zhukov, V A Gubanov, O Jepsen, N E Christensen, O K Andersen *Philos. Mag.* **58B** 139 (1988)
106. V P Zhukov, N I Medvedeva, V A Gubanov *Phys. Status Solidi B* **151** 407 (1989)
107. G G Shveikin, N I Medvedeva, A L Ivanovskii *Neorg. Mater.* **32** 52 (1996)
108. N I Medvedeva, A L Ivanovskii *Zh. Neorg. Khim.* **41** (1996) (in the press)
109. M V Kuznetsov, E V Shalaeva, S V Borisov, B V Mitrofanov, A L Ivanovsky, G P Shveikin *Mendeleev Commun.* 94 (1995)
110. M V Kuznetsov, S V Borisov, E V Shalaeva *Thin Solid Films* (1996) (in the press)
111. J Redinger, P Marksteiner, P Weinberger *Z. Phys. B, Condens. Matter* **63** 321 (1986)
112. P Marksteiner, P Weinberger, A Neckel, R Zeller, H Dederichs *J. Phys. F, Met. Phys.* **16** 1495 (1986)
113. P Pecheur, G Toussaint, E Kauffer *Phys. Rev. B, Condens. Matter* **29** 6606 (1984)
114. W E Pickett, B M Klein, R Zeller *Phys. Rev. B, Condens. Matter* **34** 2517 (1986)
115. W Jeitschko, H Nowotny *Monatsh. Chem.* **98** 329 (1967)
116. J J Nickl, K K Schweitzer, P Luxenberg *J. Less-Common Met.* **26** 335 (1972)
117. T Goto, T Hirai *Mater. Res. Bull.* **22** 1195 (1987)
118. A L Ivanovsky, D L Novikov, G P Shveikin *Mendeleev Commun.* 90 (1995)
119. L T Huetter, H H Stadelmaier *Z. Met.kd.* **41** 230 (1950)
120. R Butters, H P Myers *Philos. Mag.* **46** 895 (1955)
121. M L Swansoa *Can. J. Phys.* **40** 719 (1962)
122. H H Stadelmaier, L J Huetter *Acta Metall.* **7** 415 (1959)
123. D Fruchart, E F Bertaut, B Le Clere *J. Solid State Chem.* **8** 182 (1973)
124. J Schoebel, H H Stadelmaier, G Lorthioir, E Fruchart, R Fruchart *Z. Met.kd.* **55** 378 (1964)
125. M Haschke, H Nowotny, F Benesovsky *Monatsh. Chem.* **98** 273 (1967)
126. W Jeitschko, H Nowotny, F Benesovsky *Monatsh. Chem.* **95** 436 (1964)
127. H H Stadelmaier, A Fraeker *Z. Met.kd.* **53** 48 (1962)
128. H H Stadelmaier, T Yun *Z. Met.kd.* **52** 477 (1961)
129. D Fruchart, E F Bertaut, R Madar, G Lorthioir, R Fruchart *Solid State Commun.* **9** 1793 (1971)
130. E F Bertaut, D Fruchart *Int. J. Magn.* **2** 259 (1972)
131. D Fruchart, E F Bertaut, J P Senateur, R Fruchart *J. Phys. Lett.* **38** 21 (1977)
132. D Fruchart, E F Bertaut *J. Phys. Soc. Jpn.* **44** 781 (1978)
133. D Fruchart, J P Bouchand, E Fruchart, G Lorthioir, R Madar, A Ronault *Mater. Res. Bull.* **2** 1009 (1967)
134. E F Bertaut, D Fruchart, J P Bouchand, R Fruchart *Solid State Commun.* **6** 251 (1968)
135. M Barberon, E Fruchart, R Fruchart, G Lorthioir, R Madar, M Nardin *Mater. Res. Bull.* **7** 109 (1972)
136. M Barberon, R Madar, E Fruchart, G Lorthioir, R Fruchart *Mater. Res. Bull.* **5** 1; 903 (1970)
137. S Nagakura, K Tanehoski *J. Phys. Soc. Jpn.* **25** 840 (1968)
138. R Fruchart, R Madar, M Barberon, E Fruchart, G Lorthioir *J. Phys. Colloq.* **32** 982 (1971)
139. T Kaneko, T T Kanomata, K Shirakava *J. Phys. Soc. Jpn.* **56** 4047 (1987)
140. E Kren, G Kadar, L Pal, J Solyon, P Szabo, T Tarnorzi *Phys. Rev.* **171** 574 (1968)
141. T Kaneko, T Kanomata, S Hiura, G Kido, Y Nakagawa *J. Magn. Magn. Mater.* **70** 261 (1987)
142. T Kanomata, T Kaneko, Y Nakagawa *J. Solid State Chem.* **96** 451 (1992)
143. J P Jardin, J Labbe *J. Phys.* **36** 1317 (1975)
144. J P Jardin, J Labbe *J. Appl. Phys.* **52** 3 (1981)
145. J P Jardin, J Labbe *J. Solid State Chem.* **46** 275 (1983)
146. K Motizuki, H Nagai *J. Phys. C, Solid State Phys.* **21** 5251 (1988)
147. K Motizuki, H Nagai, T Tanimoto *J. Phys. (France)* **49** 161 (1988)
148. A L Ivanovskii, I S Elfimov, A N Skazkin, V M Zhukovskii, G P Shveikin *Fiz. Tverd. Tela* **37** 3738 (1995)
149. A L Ivanovskii *Zh. Neorg. Khim.* **41** (1996) (in the press)
150. M Shirai, Y Ohata, N Suzuki, K Motizuki *Jpn. J. Appl. Phys.* **32** 250 (1993)
151. S Ishida, S Fujii, M Maeda, S Asano *Jpn. J. Appl. Phys.* **32** 248 (1993)
152. S Ishida, S Fujii, A Sawabe, S Asano *Jpn. J. Appl. Phys.* **32** 282 (1993)
153. T Kaneko, T Kanomata, in *Recent Advances in Magnetism of Transition Metal Compounds* (Eds A Kotani, N Suzuki) (Singapore: World Scientific, 1993) p. 103
154. T Kaneko, T Kanomata, K Shirakawa *J. Phys. Soc. Jpn.* **44** 781 (1978)
155. C A Kuhnen, A V dos Santos *Solid State Commun.* **85** 273 (1993)
156. C A Kuhnen, A V dos Santos *J. Magn. Magn. Mater.* **130** 353 (1994)
157. K Tagowa, E Kita, A Tasaki *J. Phys. Soc.* **21** 1596 (1982)
158. D Andriamandroso, L Fefiliatiev, G Demazeau, L Fournes, M Pouchard *Mater. Res. Bull.* **19** 1187 (1984)
159. G Ertl, M Nuber, N Thiele *Z. Naturforsch. A, Phys. Sci.* **34** 30 (1979)
160. S Matar, P Mohn, G Demazeau, B Siberchicot *J. Phys. (France)* **49** 1761 (1988)
161. Wei Zhou, Li-jia Qu, Q Zhang, D Wang *Phys. Rev. B, Condens. Matter* **40** 6392 (1989)
162. C A Kuhnen, R S de Figueiredo, V Drago, E Z da Silva *J. Magn. Magn. Mater.* **111** 95 (1992)
163. G Demazeau, D Andriamandroso, M Pouchard, B Tanguy, P Hagenmuller *C. R. Seances Acad. Sci. II, Mech.-Phys. Chim. Sci.* **297** 843 (1983)
164. U K Poulsen, J Kollar, O K Andersen *J. Phys. F, Met. Phys.* **6** L241 (1976)
165. O K Andersen, S Madsen, U K Poulsen, O Jepsen, J Kollar *Physica B* **86–87** 249 (1977)
166. D M Roy, D G Pettifor *J. Phys. F, Met. Phys.* **7** L183 (1977)
167. J Kubler *Phys. Rev. Lett.* **81A** 81 (1981)
168. C A Kuhnen, E Z da Silva *Phys. Rev. B, Solid State* (1996) (in the press)